DETERMINATION OF NATURAL RADIOACTIVITY LEVELS AND RADIOLOGICAL HAZARDS OVER ILESHA AND ENVIRONS USING AIRBORNE RADIOMETRIC DATA

BY

OLOJEDE, DARE SAMSON
20PGCG000167

A DISSERTATION SUBMITTED TO THE DEPARTMENT OF PHYSICAL SCIENCES, COLLEGE OF PURE AND APPLIED SCIENCES,

LANDMARK UNIVERSITY, OMU-ARAN, KWARA STATE.

IN PARTIAL FUFILMENT OF THE REQUIREMENT FOR THE AWARD OF MASTER OF SCIENCE (M.Sc.) DEGREE IN PHYSICS.

SEPTEMBER, 2022

DECLARATION

I, Dare Samson OLOJEDE, M.Sc. student in the Department of Physical Sciences, Physics Programme, Landmark University, Omu-Aran, hereby declare that this dissertation entitled “Determination of Natural Radioactivity Levels and Radiological Hazards over Ilesha and Environs Using Airborne Radiometric Data”, that I submitted is my genuine research. Material(s) that I got from other work sources done by persons or institution has acknowledged appropriately.

OLOJEDE DARE SAMSON _____

20PGCG000167 Signature & Date

CERTIFICATION

This is to certify that this dissertation has been read and approved as meeting the requirements of the Department of Physical Sciences, Landmark University, Omu-Aran, Nigeria, for the Award of Master of Science Degree in Physics.

_____ _____

Prof E. B. Faweya Date

(Supervisor)

_____ _____

Dr S. O. Ikubanni Date

(Co-Supervisor)

_____ _____

Dr S. O. Ikubanni Date

(Ag. Head of Department)

_____ _____

Prof M. O. Isinkaye Date

(External Examiner)

DEDICATION

I dedicate this dissertation to the all sufficient God, the Father of light with whom there is no variableness or shadow of turning, my Lord and Saviour Jesus Christ and the Holy Spirit the Guide of my youth (James 1:17)

ACKNOWLEDGEMENTS

All the glory be to the almighty God who created the heavens and the earth, He spared my life and made a way for this work. He is worthy to be praised all the way.

I appreciate my supervisor, Professor Ebenezer Babatope FAWEYA and my co-supervisor, Dr Stephen O. Ikubanni for their relentless effort to see this research done, done well and as at due time. I cannot thank you enough Sirs, you are indeed a blessing.

I want to appreciate my lecturers Professor Jacob Adeniyi who taught me Electromagnetic Theory and Research Methodology in Physics, Dr Adebiyi who taught me Physics Electronics, Dr Onate who taught me Quantum Physics and Dr Salawu who taught me Mathematical Physics. The efforts of Professor Babatunde Adebesin, Dr Olajumoke Iyinbor, Dr Adewunmi, Dr Falade, Dr Dada, Pastor Dopamu, Mr Adebiyi, Mr Olanrewaju, Physics program, Physical Sciences Department and College of Pure and Applied sciences, School of Postgraduate Studies staffs and faculty are of immense support; I have a good impression to have met you.

I want to appreciate my wife, Dr Ayoyinka Olojede who received this degree from above and by faith despite my fears of inconveniences it could pose to us as a family; you ensured my maiden publication in the sciences was to time amidst all odds. Thank you for been lovely and a help meet indeed.

ABSTRACT

The quest to know the health implications of certain ingestible and digestible in the environment on humans is on the increase. Unique and related researches in Ilesha have been carried out except for coverage of health risk to the populace in the neighbouring villages and towns which may be due to security challenges and simile unprecedented exposure of expatriate to excess radiation. This work was to determine rocks' radioactivity levels, radioactive heat generation rate and surrounding radiation hazards to humans using airborne radiometric data. The mean concentration of the radioelements and activity concentration of Ilesha and environs were 2.66 %, 16 ppm and 13.98 ppm, and 831.35, 56.77 and 56.77 Bq kg^{-1} for ^{40}K, ^{232}Th and ^{238}U, respectively.

The estimated average radioactive heat production (A) for the studied rocks of 2.03 μWm^{-3} was above the world crustal mean range with values from 0.8 μWm^{-3} to 1.20 μWm^{-3} which may lead to enhanced average temperature of the area studied. The average absorbed dose of 52.60 nGy h^{-1} is consistent with the world standard range, and other investigated radiological variables, which include the outdoor and indoor effective dose for a year, external and internal hazard indices, gamma representative index and activity utilization index were all found to be below the recommended world minimum of 1.00 mSv y^{-1} for the rocks. Furthermore, the estimated gonadal effective dose for a year (362.30 $\mu Sv\ y^{-1}$) and excessive lifetime cancer risk (9.00×10^{-4}) which were above the world permissible limits are indications to the fact that banded gneisis, migmatite, porphyritic granite and quartzite rocks of the studied area with high gamma radiations are not advisable for use in construction works and other applications. Moreover, the regular check on the radiological threat state of the studied area is proposed.

Radioactivity Levels, Gamma Radiations, Airborne Radiometric Data, Radiological Hazards, Radioactive Heat

Word count: 293 words

TABLE OF CONTENTS

LIST OF TABLES

LIST OF FIGURES

CHAPTER ONE

1.0 INTRODUCTION

1.1 Background to the Study

The term “health” is not just a condition of whole mental, physical and social well-being but also being free of disease or infirmity (Tallini, 2011). Certain activities like smoking, burning of fossil fuels, mining, agriculture, as well as natural and artificial radioactivity has been identified to pose risk to human health (Weldeslassie *et al*., 2018; Madhav *et al*., 2020). Threats to health in form of lung cancer, fever, loss of hair, gene pool damage, mental retardation, blood cancer and even death have all been linked to extended exposure (beyond permissible limits) to radiations from natural sources (Semennova *et al*., 2020).

Rocks in Ilesha and environs have been found to be rich in radioactive elements like uranium, thorium and potassium (Oyinloye, 2006). Uranium, potassium and thorium are the three primary radioelements that make up natural radionuclides. They can be found in varying amounts in the minerals of crustal rocks such as granite, gneiss, shale, and basalt, as well as in the by-products of their weathering. These radioactive elements emit gamma and x-radiations, alpha particles and beta particles, whose interaction with matter have possible health risks (Terrill, *et al*., 1954).

In assessing this effect, an essential technique for geological mapping; an airborne radiometric survey which provides information into the distribution of radio elements on the Earth's surface with the aid of a gamma ray spectrometer mounted on an airplane flown close to surface rocks and soils provides details on the characteristics of rocks and soil, particularly their natural radionuclide content, as well as the natural radioactivity levels and the consequent health effects. The survey findings are displayed as maps that show total radiation levels and the concentrations of uranium, potassium and thorium.

1.2 Statement of the Problem

Exposure to radiations for a long time beyond what is considered safe for human beings can cause diseases like lung cancer, loss of hair, fever, defects in the gene pool, offspring's' mental impairment from teratogenic radiation exposure at pregnancy, blood cancer or even death (Akingboye *et al.*, 2021).

Mining areas has been found to provide a radiological threat to the local community (Ibeanu, 2003). Gold; which is a major mineral mined in Ilesha is obtained through a series of geological processes deep under the earth's surface. In this process, certain radiations are exposed to the atmosphere of such environment and as a result, the miners, mining site, host and neighbouring acommunities could be predisposed to harmful radiations from such gold mining industries in the form of external gamma radiation from ores, inhalation of dust containing decay progenies of ^{238}U, ^{232}Th, and ^{40}K, and inhalation of radon's short-lived decay products (UNSCEAR, 2000). In the same vein, Mineral mines and their processing can also harm the environment by exposing members of the public to radiation through improper drilling, leaching, handling, storage, and transportation of mineral ores and waste media (Innocent *et al.*, 2013). Due to the health risks associated with exposure to naturally occurring radioactive materials (NORM), the gold mining practice was documented as a potential exposure basis to naturally occurring radioactive materials (Idriss *et al.*, 2018).

Ilesha-west local government area has been traditionally known for gold mining activities, which began in the early 1950s (Adesipo *et al.*, 2020). Hence, its residents and those in communities around it may be at risk of potentially harmful radiations. The assessment of the risk to the health of residents in this area with airborne radiometric data is yet to be carried out.

1.3 Justification for the study

There is a growing interest to know the health implications of various substances in the human environment that includes the gaseous, liquid and

solid in the human society. Although, there have been some isolated works with focus on particular locations in the Ilesha communities, there have not been coverage of health risk to the populace in the neighbouring villages and towns due to security challenges and unprecedented exposure of expatriate to excess radiation. Hence, the need of use of the airborne radiometric data of these areas to assess the risk posed to the health of residents by gamma radiations. Positive outcome of this analysis and interpretation will inform appropriate actions as to mitigate the long-term health risk and hazard to occupants of Ilesha and environs.

1.4 Aim of the study

This study aims at determining the natural radioactivity levels and the associated radiological hazards in Ilesha and environs using airborne radiometric data.

1.5 Objectives of the study

This study has the outlined objectives:

(i) Quality analysis and interpretation of airborne radiometric data;

(ii) Estimation of radiation levels from the airborne radiometric data; and

(iii) Assessment of the health risks from the airborne radiometric data.

1.6 Scope of the study

The airborne radioelements that are most probable in the rocks are potassium (^{40}k), Uranium (^{238}U) and Thorium (^{232}Th). These elements are important to airborne radiometric data and gamma ray spectrometric survey as they help to describe radioactivity level and how it varies with rocks and locations. This work is therefore designed to make use of airborne radiometric data to assess the natural radioactivity level and the associated radiological hazards.

1.7 Significance of the study

Evaluating the airborne radiometric data is important and significant as a preliminary investigation of the adverse health effects on the environment and humans from radiations emitted from radioactive sources present in rocks and soils. This work will foster the united nations structural developmental goal (SDG) under health and hunger.

CHAPTER TWO

2.0 LITERATURE REVIEW

2.1 Fundamentals of Gamma Radiation Spectrometry

Gamma radiation spectrometry is an analytical means that enables the detection, identification and quantification of many gamma releasing radionuclides in a single sample measurement with less tasking preparation. The measurement results in a spectrum of lines that have amplitudes that are directly proportional in magnitude to the radionuclide's activity. Its placement in the horizontal axis provides information about its energy (Ali, 2015). The method necessitates taking into account, the source intensity and the source-detector geometry, both of which have an effect on the measured effluence from the gamma radiation while the source's strength and source-detector set -up influence the measured gamma radiation effluence per unit time. Other additional elements like the distribution of airborne radiation sources, vegetation non-radioactive overburden, soil moisture, and rainfall have an impact on the reported effluence rates (Syaeful *et al.*, 2014).

In this chapter, the basics of gamma radiation spectrometry are evaluated, and the chapter concludes with a summary on the use of non-complex analytical models to comprehend the physics and prior research on airborne radiometric data.

2.1.1 Gamma Radiation Sources

A photon of gamma radiation has a discreet energy that is a property of its

isotopic source. This property serves as the basis of gamma radiation spectrometry (GRS). The assessment of gamma radiation energies has application in the determination of its source. Radiations of natural sources are majorly from isotopes broken down during the generation of the planetary bodies and they have very long half-lives that ensure their existence until today. Major of the sources are: potassium (^{40}K); uranium (^{238}U and ^{235}U and their daughters), and thorium (^{232}Th and its daughters). These are the ones that generates gamma radiations of high energy and sufficient intensity that has been used in gamma radiation survey (Minty, 1997; Anusha, 2011). These gamma radiations and atomic particles of cosmic origin react with atoms and molecules in the upper atmosphere producing a complex secondary radiation that reacts with matter in the surrounding to give cosmic a gamma radiation background. The trace quantity of potassium, uranium and thorium found in the detector and instruments in the surrounding are called instrument background radiations. An example is the radiation from the helicopter in the situation of airborne mappings.

2.1.2 Characteristics of Gamma Radiation Spectra

The equivalent arrangements of potassium, uranium and thorium have unique theoretical line spectra that symbolise the energy array of photons that are from the source. The individual radioelement produces a smooth peak that shows the energy of directly transmitted photons. When this is overlapped on the spectrum of Compton scattered photons, it reveals a continuum of energy up to the maximum of the photons released by the isotope (Minty, 1997). A measured spectrum is a complex factor of many features like the source concentration with its geometry, the detector's altitude, thickness of desired non-radioactive overburden, as well as the detector's response function. Distinct samples of potassium (K), uranium (U), and thorium (Th) spectra having large integration time that would be recorded at airborne height are given below (Figures: 2.1; 2.2; and 2.3).

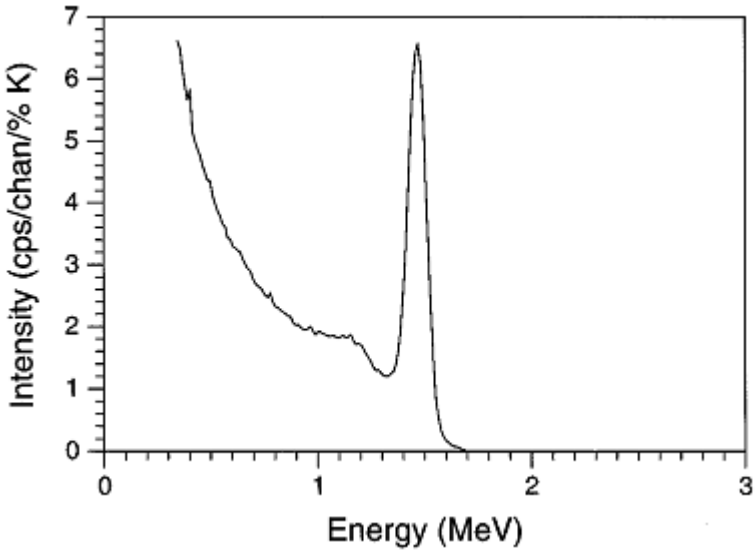

Figure 2.1: Simulated Potassium Spectrum of 100 m Altitude with a Long Integration duration (IAEA, 2003)

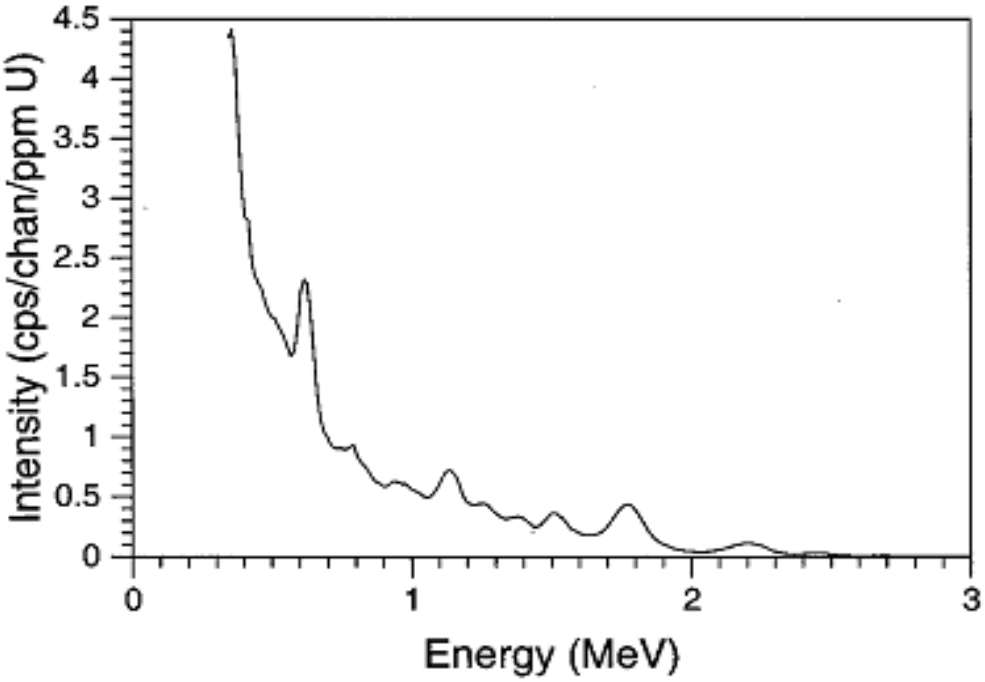

Figure 2.2: Simulated Uranium Spectrum of 100 m Altitude with a Long Integration duration (IAEA, 2003)

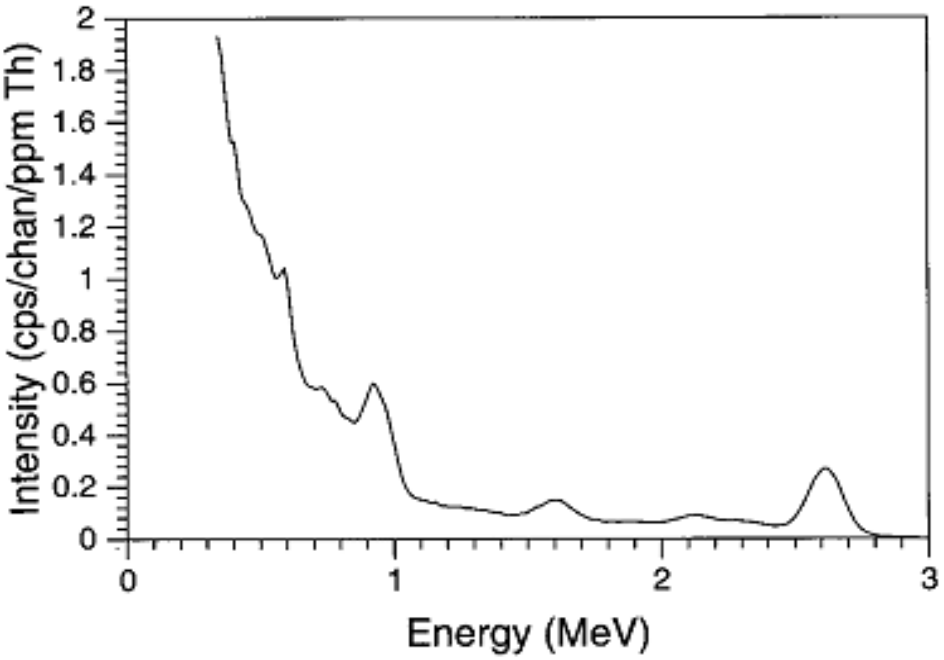

Figure 2.3 Simulated Thorium Spectrums at 100 m Altitude with a Long Integration Duration (IAEA, 2003)

2.1.3 The Detector Response

The detector is the main part of the gamma spectroscopy. Whenever the detection substances engage the photons of the gamma radiations, there is usually a change of energies to electrons or to positrons in the event of annihilation. Ionised atoms and ion pairs are made as a result of particles giving up their energy inside the space of the detector. Signal from the detector built on these auxiliary components. Hence, the most common

material used in gamma radiation spectrometry systems in the high purity germanium (Rosianna, 2020; Reguigui, 2006).

Gamma radiations are usually detected using Thallium doped sodium-iodide (NaI(Tl)) scintillation crystals in airborne gamma radiation spectrometry. One or more very energetic electrons are produced as a consequence of the scattering and absorption process of an inclined gamma radiation photon inside the detector crystal. The distinct feature of NaI(Tl) scintillation crystals is that the energy given to the electrons is changed into a burst of light (Minty, 1997; IAEA, 2003). The airborne gamma radiation detector significantly alters the spectra. The key part of the detector response are the detector efficiency as a factor of energy, proportional sensitivity, resolution, dead time, with variables influencing how a spectrometer measures a real pulse height spectrum (Minty, 1997).

2.1.4 Source Detector Geometry

The efficiency factor of the source detector is influenced by the size, distance and density of the detector. The shape of the observed spectrum is influenced by both source type and thickness. Material between the source and the detector, as well as inside the source, attenuates radiation coming from the ground. Adding the source-detector distance or increasing cover, reduces the overall flux at all energy levels. It's also significant how detector height affects total flow (Minty, 1997; IAEA, 2003; Reguigui, 2006).

2.2 Interaction of Gamma Radiations with Matter

Gamma radiations are made up of a flow of elementary particles and energy quanta. They can be categorized by their physical characteristics and energy. These characteristics and energy controls how they interact with the material. Their three means of interacting with matter atoms are the photoelectric effect, Compton effect and the pair production (Minty, 1997; Abdo *et al.*, 2009). For lower energies, the photoelectric effect predominates and causes a

gamma quantum's whole energy to be absorbed when it collides with an atom's electron. At moderate energies, Compton scattering dominates and is caused by an electron colliding with an incoming photon. The incident photon is scattered at such an angle that is inclined to its initial path and loses some of its energy to the electron. For energies above 1.02 MeV, pair production, a phenomenon by which an incident photon is totally absorbed to give up a pair of electron and positron in a nucleus' electric field takes place. The cross-section which represents the likelihood of a photon mixing up with matter relies on the matter's composition in conjunction with the photon energy, E. The correlation between the scattering and absorption activities, incident photon energy, and absorbing material atomic number is shown in Figure 2.4. Compton effect is the main interaction process for matter made up of rock, water, and air when it comes to gamma radiation with energy of about 2.615 MeV that are from natural terrestrials. Every radiation detector's operation is dependent on the factor of how the radiation to be detected interacts with the detector's substance. Hence, knowledge of the basic processes by which radiation interacts with matter and loses its energy must be the foundation for comprehension of the response of a particular type of detector. Gamma radiations can theoretically be absorbed or scattered via a number of techniques. Both the photon's energy and the material's atomic number (Z) play a significant role in the processes.

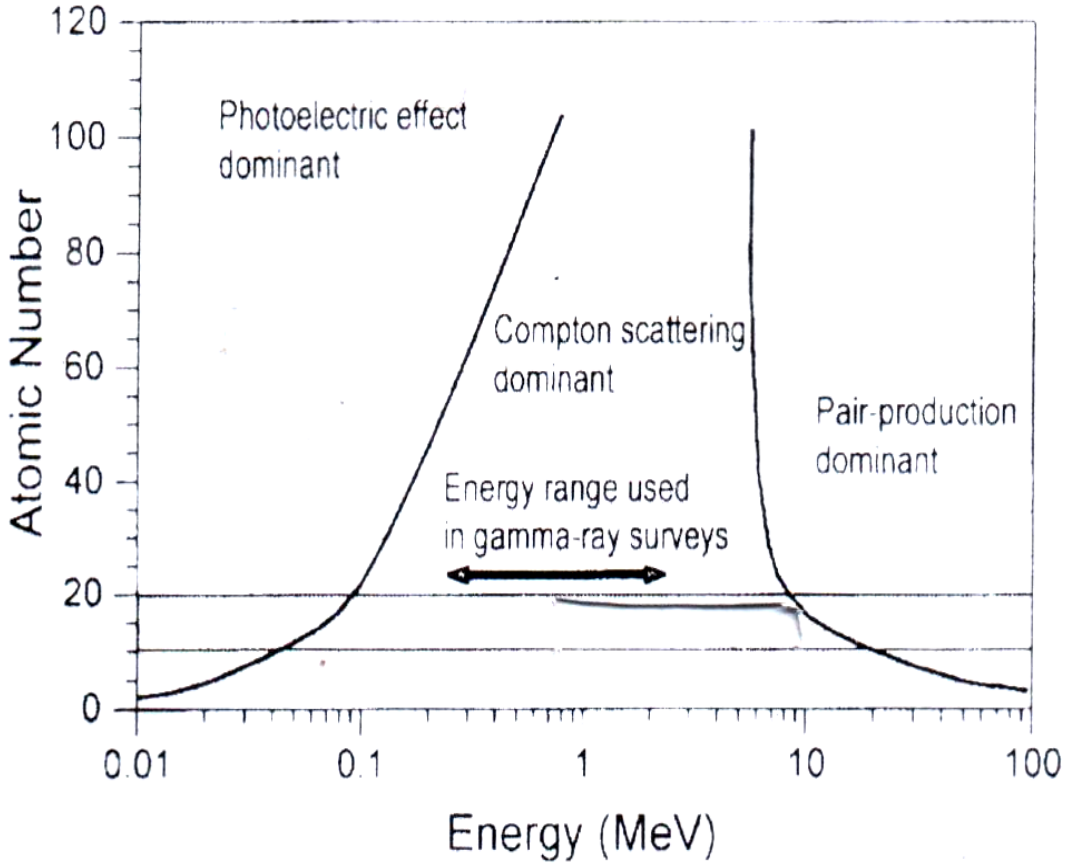

Figure 2.4: The graph of the three processes of Interaction of γ- Radiation with Matter (IAEA, 2003)

2.2.1 Photoelectric Effect (P.E.)

Photoelectric effect (P.E.) is that interaction process in which a photon of energy hυ collides with an inner shell electron (K, L, M, N shells) imparting energy to it as presented in Equation 2.1. This energy overcomes the electron's binding energy and it is lost by the atom. The electron that is removed is called the photoelectron. Photo-electrons acquire kinetic energy and the space left in the inner shell would be occupied by cascading of electrons from higher energy levels which amounts in emitting characteristic X-radiations. The energy conservation technique requires that:

$$h\nu = \Phi + Ee \qquad 2.1$$

Where Φ is the electron's binding energy and Ee is the electron's kinetic energy in joules.

Gamma rays (or X-rays) of relatively low energy interact mostly through this photoelectric mechanism; the procedure is improved for absorber materials with high atomic number (Z). The important electrons in P.E. are those that are more closely bonded. When the photon has the exact energy to release the bound electron, then the absorption process is enhanced. This is called Resonance Absorption. The predominance of high atomic number materials like lead in gamma radiation shields is mostly due to the significant dependence of the photoelectric absorption probability on the absorber's atomic number (Rizwan, 2015; Achola, 2009). In soft tissue, P.E is a total absorption process because the binding energy of the K-shell is low, approximately equal to 0.5 keV and the characteristic X-radiation emitted will be absorbed within the same cell (Boone, 2000).

2.2.2 Compton Effect (C.E.)

The process of interaction that takes place at intermediate photon energy levels (hυ > 50 keV) is the Compton effect also known as the Compton scattering. In this technique, a photon releases a portion of its energy to a 'free' electron which recoils at angle Φ. This electron is referred to as the Compton electron. The scattered photon at angle θ recedes from the collision with energy, hυ' less than that of the incident photon. Energy conservation requires according to the Equations 2.2, 2.3 and 2.4 that:

$$h\nu = \Phi + h\upsilon' \qquad 2.2$$

The increase of wavelength value called Compton shift is represented by:

$$\Delta\lambda = \lambda^{1} - \lambda = \frac{h}{m_0 c}(1 - \cos\theta)$$

2.3

The gamma radiation has an energy represented by:

$$h\nu^{1} = \frac{h\nu}{1 + \frac{h\nu}{m_0 c^2}(1 - \cos\theta)} \qquad 2.4$$

Where the rest mass energy ($m_o c^2$) is 0.511 MeV.

The quantity of electrons accessible at scattering targets predicts the likelihood of Compton scattering per atom of the absorber, the chance rises directly with increasing atomic number Z.

2.2.3 Pair Production

In pair production, a positron-electron pair is made at a location close to the nucleus. An electron is ejected from an energy state below zero into an energy state above zero during the formation resulting in an anti-matter positron. A hole is left behind where the energy state below zero would normally be filled, the hole is the positron. Although the hole has a positive charge, it exhibits all the characteristics of an electron. Minimum photon energy of 1.02 MeV is needed to generate a pair of electron and positron. The photon is a boson of

spin unity and angular momentum zero. But an electron and a positron will not have angular momentum of zero. The creation must therefore be in the vicinity of a nucleus so that the conservation laws hold and the nucleus must have absorbed the excess angular momentum, it is for this reason that we do not see an arbitrary creation of pairs whenever there is intense radiation. If the photon is completely absorbed but its energy is in excess of 1.02 MeV, the balance of energy is changed into kinetic energy for the particles according to Equation 2.5.

$$h\upsilon = 2mc^2 + ke^- + Ke^+$$

2.5

Where h is the Planck's constant and υ is the frequency of the radiation.

All the three processes may take place simultaneously; the total attenuation coefficient μ is given by Equation 2.6.

$$\mu = \tau_{P.e} + \sigma_{compton} + k_{pair\ production} \qquad 2.6$$

Figure 2.4 provides an easy way to see the relevance of the three processes for various absorber medium and gamma radiation energy. According to the absorber Z, the left line shows the particular energy for Compton scattering and photoelectric absorption are proportionately likely to take place. The specific energy at which Pair production and Compton scattering are proportionately likely to occur is shown by the line to the right. Thus, in the figure, three regions identify where photoelectric absorption, Compton scattering, and pair production occurs.

2.3 Measurement of Gamma Radiation

The information in the energy range of 0.0 - 3.0 MeV is acquired by a contemporary gamma radiation spectrometer in 256 or 512 channels. Each channel records every gamma radiation that the detector absorbs and has energy value around 11.7 keV range. Ordinarily, counts per second are modest. During a one-second counting interval, an aerial gamma radiation spectrometer filled with 32 litres of sodium iodide (NaI) detectors may likely read one or even zero counts in certain large energy channels. The accuracy

at which a spectrometer could determine the gamma radiation energy is called the energy resolution of the spectrometer (ERS). The ERS is calculated as a percentage of the photo-peak energy represented as the complete width of a photo-peak at half the greatest amplitude. For large volume NaI detectors, the typical spectrometer resolutions are 10 per cent for ^{137}Cs at 0.662 MeV and 7 per cent for ^{208}Tl at 2.61MeV. The standard method for collecting and analysing gamma radiation spectrometric data involves keeping an eye on 3 to 4 rather large spectral windows according to Figure 2.5. Monitored by the window of the K energy are the 1.46 MeV gamma radiations that ^{40}K emits. Gamma radiation disintegration outcomes in the uranium and thorium decay series are tracked by the uranium and thorium energy windows. These windows have been found to be the best for measuring potassium, uranium and thorium activity. Total radioactivity is measured via the total-count window (IAEA, 2003). A typical airborne gamma radiation spectrum is shown in Figure 2.5.

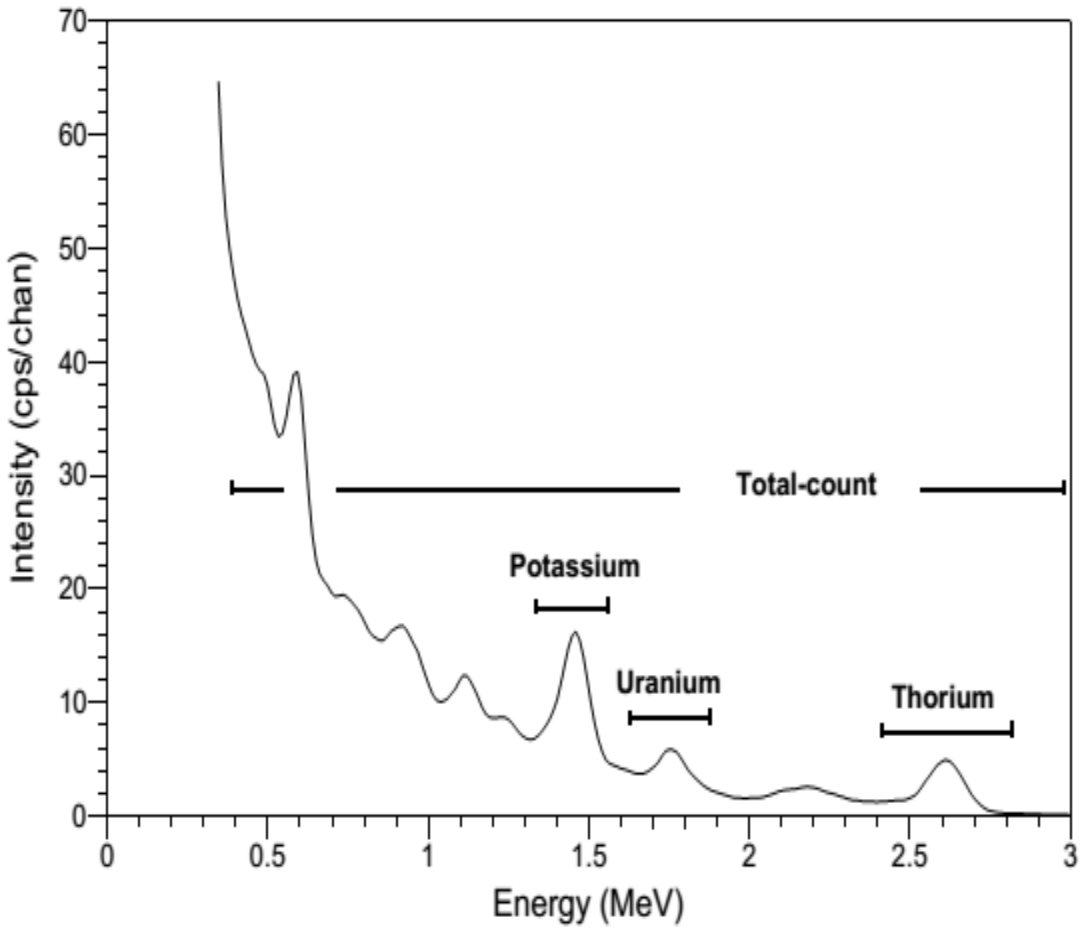

Figure 2.5: Representative Airborne Gamma Radiation Spectrum graph that shows the position of the conventional Energy Windows (IAEA, 2003)

2.4 Airborne Gamma Radiation Spectrometry for Natural Radioelement Mapping

According to Table 2.1, gamma radiation surveys are used to find where minerals like gold, tin and tungsten are in their raw state. The activity of mineralisation is often done by metasomatism of potassium, potassium, uranium and thorium concentration maps in the rocks and soils to enhance geological activities, background radiation to provide a benchmark against which man-made pollutants can be estimated (IAEA, 1991).

2.4.1 Survey Methodology

The survey variables that are put into consideration in gamma radiation spectrometry are the line spacing, crystal volume, fieldwork operational protocol and auxiliary instrumentation. To map radioelements in their raw state, the focus of the flight line, if known, should be at 90^{o} to the geological outfit of interest, frequently the geological strike. In treacherous alpine terrain, when conventional grid flying is unpredictable or impractical, flying is occasionally accomplished by outlining the contours of the landscape. The flight lines more often than not are in the same direction with the long axis of the zone of interest when seeking for radioactive objects (IAEA, 1991).

The flight line spacing is dependent on a number of things like the available money, the need to cover a broad area and the tolerance for a little unpredicted situation. One kilometre line spacing is the usual when it comes to geological reconnaissance. In comprehensive uranium surveys, line spacing could be as small as 100 meters if the flying altitude is 100 meters or below. A point source anomaly's decrease with distance must be taken into consideration. Spectrometer surveys are usually flown at a relatively fixed altitude above the ground. Flying altitude above ground level for natural radioelement mapping with fixed wing aircraft has been roughly standardized at 120 m. Navigation is done using a compilation of electronic technologies like Doppler radar, inertial position fixing, GPS satellite fixing, or radio triangulation in addition to visual means like maps or photomosaic marked

with the anticipated flight lines locations (IAEA, 1991).

2.4.2 Calibration Data Requirements

Large height aircraft/cosmic background flight and ground calibration using radioactive pads are both necessary for converting the airborne data to ground concentrations of potassium, uranium, and thorium (IAEA, 1991).

2.4.2.1 High-Altitude Aircraft/Cosmic Background Flight

In all spectral windows, the cosmic radiation count rates rise exponentially with height above mean sea level. It is possible to figure out and use this exponential function to adjust the data for variations in cosmic rays with height above sea level. The ideal cosmic window records all incident particles with energies greater than 3 MeV, such as high-energy gamma radiations. The counts per second in the cosmic radiation window are then linked with cosmic radiation counts in different spectral ranges. To avoid the effects of terrestrial ray and the effect of radon disintegration outcomes in the surrounding air, cosmic calibration flights over land should be conducted at not less than 1500 metres beyond the level of study ground (IAEA, 1991).

2.4.2.2 Ground Calibration using Radioactive Pads

Since the spectra of potassium (K), uranium (U), and thorium (Th) overlap, individual element's window counts per second is adjusted to see the impacts of the other elements using empirically derived stripping ratios. The stripping ratios are calculated using measurements over concrete calibration pads with specifications of 1 metre x 1 metre x 0.3 metre and known concentrations of the radioelements. There are four pads needed, anomalous quantities of potassium, uranium, and thorium are present in three of such pads and the backdrop pad is the fourth one. The calibration is affected by the sample accumulation time, which is about 10 minutes. It is easiest to carry out the calibration while the detector is positioned inside the aircraft, with each pad being inserted in turn underneath the detector beneath the aircraft's belly. If there are two detectors, doing calibration of each is advised, and the measurements should be halved. It might not always be feasible to calibrate the detectors mounted on the aircraft. The detector package can be set

directly on the calibration pads in this situation to carry out the calibration. Due to the unintentional summation of certain of these gamma radiations having ^{208}Tl at 0.583 MeV, this method causes a drop in the ^{208}Tl photo-peak counts per second at 2.61MeV. These gamma radiation events are eventually added together and included in the cosmic (>3.0 MeV) count rate. The rise in the cosmic window counts per second as the thorium (Th) source is employed can therefore be noted and added to the Th window count rate to roughly account for this effect. The thickness of attenuating substance in the aircraft base is also taken into account when calculating the stripping ratios in this manner. Calibration pad architecture and composition must be properly thought out (IAEA, 2003)

2.4.3 Calibration Range Flights

The methods that have been applied in monitoring radiations of atmospheric background include flying at great height above the ground level to minimise the impacts of ground radiation, typically of value 700 metres above ground level, flying over water at survey height before and after daily flight or during the survey rounds, flying the same test line at survey height near the helicopter boundary of operations, and using upward-looking detectors (IAEA, 1991).

2.4.3.1 Radon Background Calibration Flights

The main impact of radon on the surrounding air is an enhancement in the counts per second of the U windows that look up and down as well as the overall count window. The calculated airplane backgrounds will be very high when radon is present; this is as a result of the proportional association that the cosmic and uranium windows deviates with reduced elevations. It is thus frequently possible to identify the problem of radon contamination (IAEA, 1991).

2.4.3.2 Survey Monitoring Procedures

The detection limit is determined by the technology being utilized, the survey quantities and the ground concentration of naturally occurring gamma radiation sources, as most artificial nuclides may be separated from naturally

occurring nuclides. The purpose of survey monitoring techniques is to guarantee the highest possible quality of the unprocessed airborne gamma radiation spectrometric data collected in the course of survey activities. This necessitates that the aerial gamma radiation spectrometer be properly calibrated and working. Additionally, the climate must be favourable for airborne operations (IAEA, 1991; IAEA, 2003).

2.5 Previous Work on Airborne Radiometric

Akingboye *et al.* (2021) assessed the basement complex rocks of Akungba-Akoko, South-west Nigeria with the aid of ground gamma radiation spectrometry (GRS). The ascending order of the rocks was found to be from charnockite, migmatite, granite, banded gneiss, pegmatite, to biotite granite (Ch, M, GGN, BGN, P, BG). It was discovered that the concentration of the radioelements and their corresponding activity concentrations for the study area have values 2.66 per cent, 3.16 ppm and 13.98 ppm, and 831.35, 39.01 and 56.77 Bq kg^{-1} for ^{40}K, ^{238}U, and ^{232}Th, in succession. The average value of 2.03 Wm^{-3} of radiogenic heat production (RHP) which is higher than the crustal mean range of values from 0.8 Wm^{-3} to 1.2 Wm^{-3} could appreciably increase the heat value of the studied area. The effective doses for a year, hazard indices, gamma radioactivity, and radioactivity utilization index estimated were well below the permissible limit of 1 $mSvy^{-1}$ for rocks in the area. The mean absorbed dose per second of 87.98 nGy h^{-1} has value in boarder of the acceptable range. The increased life cancer risk (1.511×10^{-3}) and gonad dosage equivalent for a year (618.874 μSv y^{-1}). However, It was advised that the pegmatitic and biotite rich rocks of the examined area have to be used less frequently due to their high gamma radiation levels. So, it was suggested that the research area be monitored from time to time.

Aisabokhae and Adeoye (2020) statistical parameters revealed the state of the radioelement concentrations within the Precambrian basement complex in North-West Nigeria. In their work, they estimated the radioactive absorbed dose of different rock units of the study area. The order of the radioelement contributing percentages for the entire rock unit under study was found to be $^{40}K > ^{232}Th > ^{238}U$.

In the work of Asere & Sedara (2020), the natural radioactivity succession, effect of radiogenic heat generation, and radiological health threats to occupants in the study location was done. A gamma radiation spectrometer was applied to estimate radiation from radioelements within and without five sets of quarry sites of Ondo State of Nigeria. The mean radioactivity values of ^{238}U, ^{232}Th, and ^{40}K were discovered to be 47.09 ± 7.49, 95.02 ± 14.11 and 1118.68 ± 126.94 Bq kg^{-1} , respectively inside quarries and 35.76 ± 7.83, 83.17 ± 11.85 and 959.71 ± 96.43 Bq kg^{-1} , respectively outside quarries. For all of the quarries, the predicted total heat output and heat flow values ranged from 0.97 to 5.37 μWm^{-3} and from 7.63 to 42.12 mWm^{-2} , respectively. The highest concentration was that of 43.5 ppm thorium and 10.4 of uranium. The average values of some estimated hazard indices have values lower than the globally permitted levels. This imply that those who operate in granite quarries, use granite products, and members of the general public who live nearby are not at risk for radiological health problems. The Johnson quarry was determined to have the greatest uranium content, total heat output, and heat flow values from a radiogenic and thermal modelling point of view, which is a property of the geological rock types and effect of high naturally occurring radioactive elements. In light of this, future investigation for prospective geothermal exploration is of the most promising uranium mineralization.

Connor *et al.* (2016) examined and evaluated previous and current work on aerial radiation monitoring in connection with the potential improvements that could be made by a joint three-dimensional radiation mapping avenues. It was discovered that a joint detailed three-dimensional topography mapping with radiation surveying has significant effect on how radiological pollutants across a site is estimated.

Adabanija *et al.* (2020) employed gamma radiation spectrometry to examine the background radiation level and radioactive heat tendencies of crystalline basement rocks in Okene, a region of southwest Nigeria that is geologically part of the crystalline basement complex, with longitudes of $6^{o}10'$ and $6^{o}19'E$ and latitude $7^{o}30'$ and $7^{o}38'N$. 19 rock samples from various locations were collected for evaluation that included the assessment ^{238}U, ^{232}Th and ^{40}K radioelements applying the Canberra S100 multi-channel evaluator with

sodium iodide detector. Banded gneiss, granite, charnockite, biotite granite, pegmatite, and schist were among the samples. Pegmatite > Charnockite > Granite > Schist > Banded gneiss > Biotite Granite was the lithological order in which the mean gamma radiation was released, and the total mean dosage was 63.35 nGy h^{-1}, or 3.11 mSv y^{-1} of effective dose equivalent per year. Banded gneiss has the largest radioactive heat tendencies, with figures ranging between 0.964 and 1.407 μWm^{-3} with a median figure of 0.964 μWm^{-3}. A minimum potential was found in biotite granite, which has a range between 0.774 and 1.014 μWm^{-3} and a mean heat production capacity up to 0.894 μWm^{-3}. The radioactive heat outcome changed as the lithology changes, and the dose equivalent for a year from background radiation was higher compared with both the natural background radiation figure (2.4 $mSvy^{-1}$) and mean value for the globe (60 nGy h^{-1}).

Gaafar *et al.* (2020) examined the mineral properties of the phosphatic rocks in the Abu Had area and complemented it with the uranium anomalies found in the air for the north portion of the area of study by a ground gamma radiation spectrometry survey. The research location in the northeast of Qena town is divided into portions by the asphalt Qena-Safaga road. 33 representative samples were collected and described from the beds. Twenty thin sections represented for phosphorites and phosphatic rocks of upper, middle and lower member of Duwi formation of the study area were prepared and examined for the identification of the mineral constituents and texture by using a polarising microscope fitted on an automatic camera and a mechanical stage. The preparation of the research area's formation was done before it was inspected for the evaluation of the elemental ingredients and nature. To ascertain the mineralogical makeup of phosphate, the unidentified minerals of phosphate rocks from the three portions of the Duwi Formation of the location were gotten, processed and evaluated in large samples using the X-ray diffraction method by a PHILIPS PW 3710/31 diffractometer, scintillation counter, Cutarget tube, and Nickel filter at 40 kilo-volt and 30 milli-ampere. An Egyptian Nuclear Materials Authority's laboratories served as the location for the mineralogical research. Consequently, the airborne uranium anomalies for the north part of the research location using a ground-based

gamma radiation spectrometry survey utilizing the RS-230 spectrometer, using a grid pattern with inherent distance of 100 metres and having an increased grid stations to around 50 metres spacing. Elemental concentration of uranium, thorium, potassium and dose per unit time surface distributions were identified, and image maps of these components were created and analyzed. According to ground gamma radiation spectrometry measurements, the research region has potassium values between 0.2 and 4.4 per cent, thorium values between 0.5 and 18 ppm, and uranium values between 0.5 and 100 ppm. The highest levels of uranium up to 100 ppm, were found in the phosphate-bearing layers of the Duwi Formation. The average effective dose rate of phosphates in the Abu Had location is 0.32 mSv y^{-1}, that is lower compared with the 1 mSv y^{-1} annual effective dose rate that is considered to be globally permitted. According to petrographic research, phosphate beds are made up of nonphosphatic particles like quartz, calcite, and pyrite embedded in silica, calcite, or iron oxide cement, as well as phosphatic particles like collophane grains and bioclasts (fragments of bone and teeth). According to XRD data, the main phosphate mineral is hydroxylapatite, and the non-phosphate minerals are calcite, quartz, gypsum, and anhydrite. The sole phosphate mineral found in the analyzed samples' phosphorites, according to the results of X-ray diffraction, is hydroxylapatite. Quartz, calcite, and gypsum were found in the sample, albeit with varying proportions. To identify radioactive nomalies and related rocks, spectrometry image maps were created and observed not just under qualitative evaluation but quantitative. Moreover, the research area's greatest concentrations of thorium and potassium, up to 18 ppm and 4 per cent, respectively, are found in Qusseir Formation. The highest uranium values, as high as 100 ppm, the lowest thorium and potassium values are found in the phosphate-bearing layers of the Duwi Formation. These results proved that large uranium concentration exists in the phosphatic layers in the Abu Had region. The phosphate-bearing beds in the Abu Had location have effective dose rates that range from 0.13 to 0.84 mSv y^{-1}, having a mean value of 0.32 mSv y^{-1} that is below the global average with value of 1 mSv y^{-1} for public exposure.

CHAPTER THREE

3.0 MATERIALS AND METHODS

3.1 Area of Study

This study location; Ilesha and environs is one of the oldest settlements in Yorubaland, located in the State of Osun, southwest of Nigeria. Ilesha and environs have Kwara state towards its north, Ondo towards its south, Ekiti towards it east and Oyo towards its west. The study location is from 7°30', 8°00'N to 4°30', 5°00'E, latitude and longitude respectively (Figure 3.1). It has a land mass of about 3025 km^2 with metropolitan census of 385,000 in 2022. Ilesha has an average elevation of 391 meters higher than the sea and a tropical atmospheric condition characterised by seasons of rain and dryness. The range of the daily average temperature is between 20 °C for really cold days and 35 °C for extremely hot days (Kayode *et al.,* 2010).

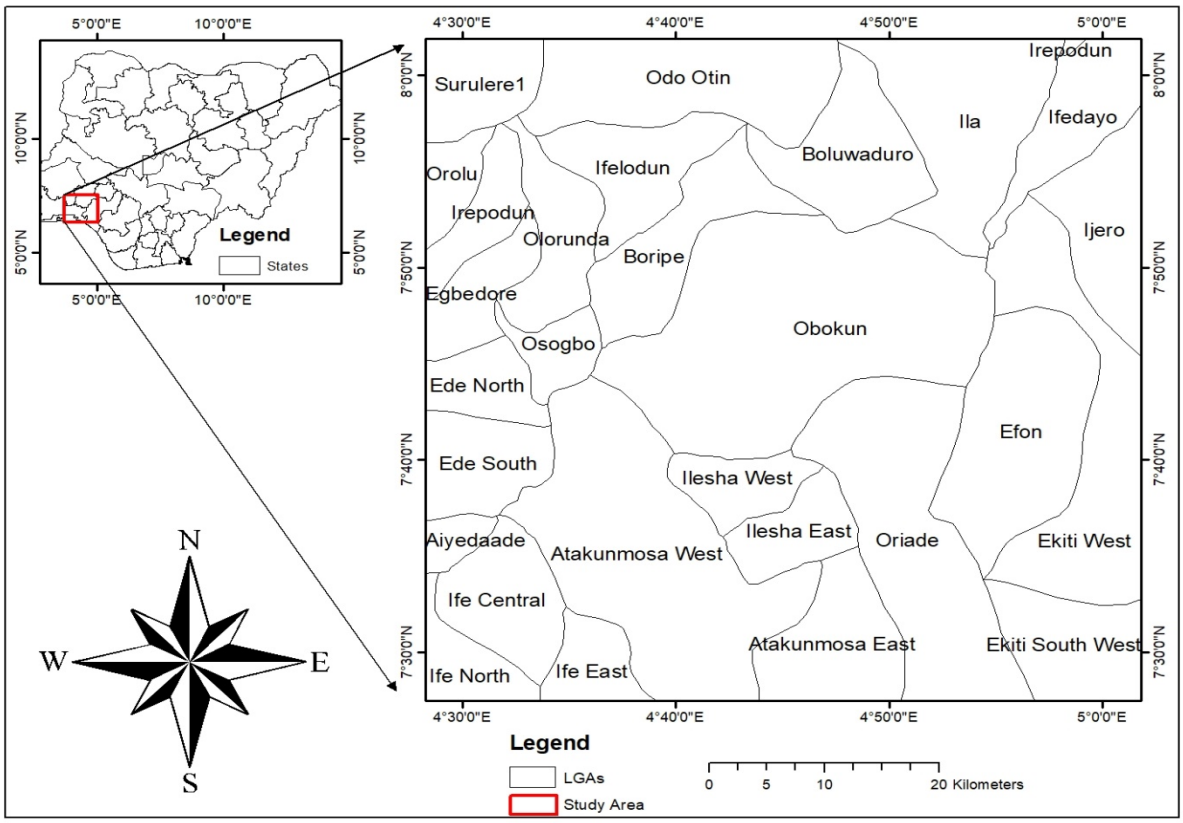

Figure 3.1: Map of Ilesha and environs, the area of study in south-west Nigeria (NGSA, 2009)

3.1.1 Geological Setting of the Area

Figure 3.2 depicts the geology of Ilesha and environs. The location is composed of Precambrian rocks expected of Nigeria's basement. The Nigerian Proterozoic schist belt, predominately formed in the west, contains the principal rock connected with the Ilesha area. The Nigerian schist belts closely resemble the Achaean Green Stone Belts in features of outlook characteristics, lithology, and mineral composition (Bolarinwa, & Adepoju, 2017). The gneiss-migmatite, amphibolites complex, meta-sedimentary formations and the intrusive suit of granite samples can all be used to categorize the rocks of the Ilesha district. Other minor rock kinds are connected to these divisions as well. Migmatites and granites, calcerous, and granulites make up the gneiss-migmatite complex. The amphibolites, amphibole schists, and small meta-ultramafites, consisting of authophillite-tremolite-chlorites and talc schist, make up mafic untramafic suit. The meta-sedimentary assemblages are primarily found as quartzites and psamitic units. Pan African granitic units make up the bulk of the intrusive suite. The primary fracture zones, commonly referred to as the Iwaraja structure located towards the east section and the Ifewara situated towards the west section, separates the schist belts formations in the Ilesha into two major parts (Akinwumiju, & Olorunfemi, 2019). The central geology map for Ilesha Schist Belt in southwest of the country is seen in Figure 3.2.

3.2 Detectors and Instruments

The instrument used in this work uses a system that comprises large sodium-iodine (NaI) crystals and gamma radiation detectors manufactured by the Black Rock Energy and Resources Trust (BGR). The detector, when strucked by gamma particles, creates feeble light pulses and the energy levels of the pulses vary depending on the kind radioelement which is determined for each pulse by photo multiplier tubes that are mounted in the detector (measured in Mega-Electron-volts, MeV). The system also comprises five crystals with total volume of 21 litres and weighing about 100 kg. The detector is installed inside

a chopper along with an electronics console. The device records a full gamma spectrum every second, with 255 channels covering the energy value from zero to three mega-electron volts in each spectrum. Sample of collected gamma radiation spectra are converted to ground concentration of potassium, thorium and uranium in ppm during data processing.

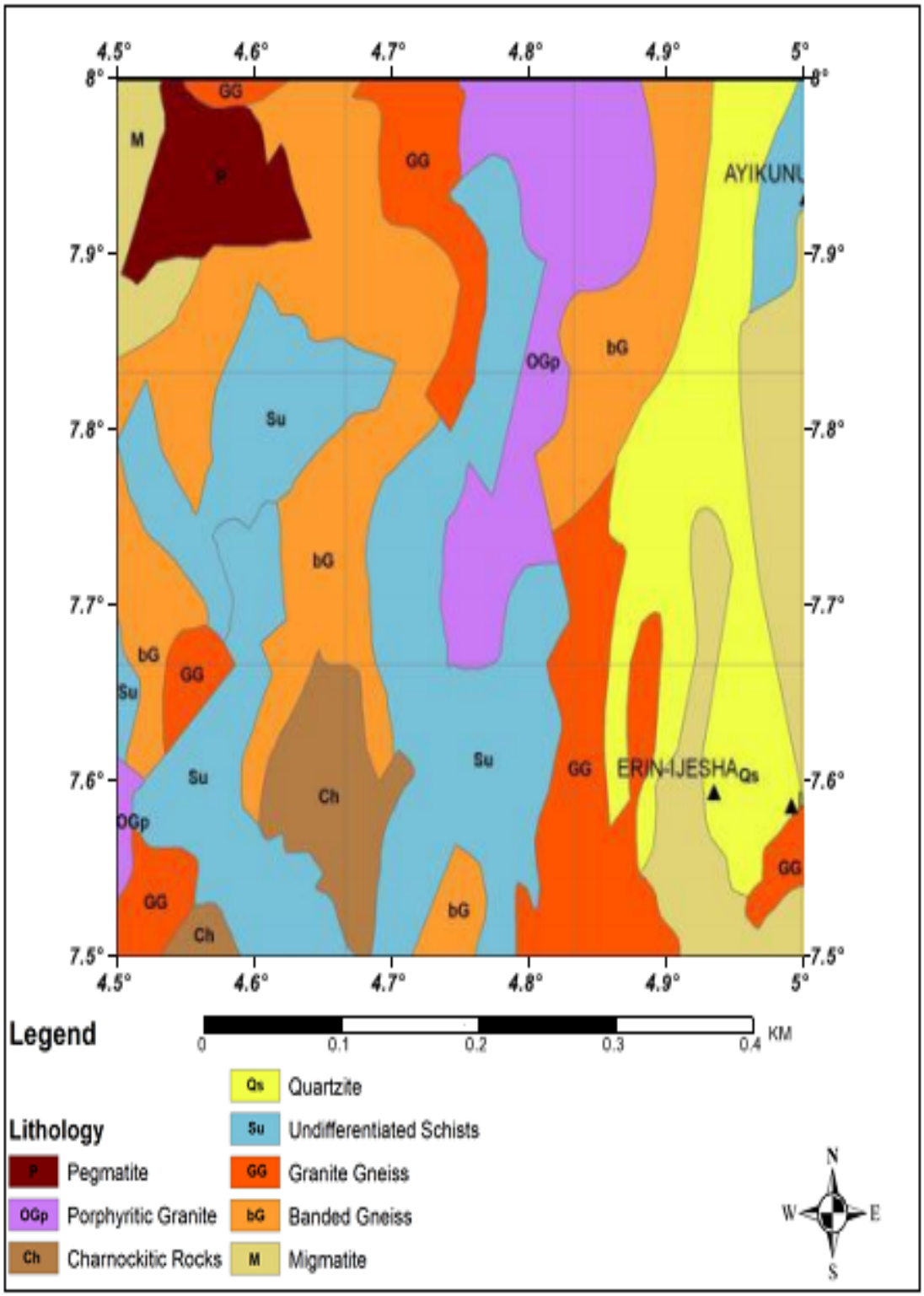

Figure 3.2: Geological map of Ilesha and environs of Osun state, Nigeria (NGSA, 2009)

3.3 Data Acquisition

The Nigeria Geological Survey Agency (NGSA), Abuja, provided airborne radiometric data used in this study. This information was gathered through a nationwide study that Fugro Airborne Survey conducted under the direction of the NGSA. The sensor average height value was 80 m, the line spacing value of the flight was 400 m, the parallel line spacing is 2000 m, and the flight line trend is 125 degrees. The radiometric data recording interval was 1 second. The barometric altimeter was ENVIRO BARO/DIGIQUARTZ, the radar altimeter was KING KR405/KING KR405B, and the data gathering system was FASDAS.

3.4 Data Interpretation

The elemental concentrations of Potassium (eK) is in percentage (%), Thorium (eTh) and Uranium (eU) with units of parts per million (ppm) were obtained from the grid and assay airborne data analysis using Geosoft Oasis Montaj. The activity concentration of the radionuclides; Potassium (A_k), Thorium (A_{Th}) and Uranium (A_U) in Becquerel per kilogram (Bq kg^{-1}) was obtained from the conversion factors presented in Table 3.1. This is for conversion from elemental concentrations in percentage and parts per million to activity concentrations in Becqurel per kilogram Bq kg^{-1} (IAEA 2003).

Table 3.1: Parameters for changing elemental concentrations in percentage (%) and parts per million (ppm) to specific activity concentrations (Bq kg^{-1}) (IAEA 2003)

Elemental Concentrations (eC)	Specific Activity Concentrations (A) (Bq Kg^{-1})
1% ^{40}K	313
1 ppm ^{238}U	12.5
1 ppm ^{232}Th	4.06

3.5 Estimation of Radiation Hazard variables

Radiation hazard was estimated with the aid of radiological standard parameters and their respective equations.

3.5.1 Dose Assessment

Equation 3.1, recommended by UNSCEAR (2000), was used to calculate the absorbed dose rate (D).

$$D\ (nGy\ h^{-1}) = 0.462A_U + 0.0417A_K + 0.621A_{Th} \quad (3.1)$$

Such that A_U, A_K, and A_{Th} are activity concentrations of uranium, potassium and thorium in Bq kg^{-1}, respectively.

3.5.2 Total Count Emission Rate (Tc)

The total count rate (Tc) which is the intensity of the radiations in nano-gray per hour (nGy h^{-1}) and counts per second (Cps) was accounted using equation 3.1.

3.5.3 Radium Equivalent Activity

The Radium Equivalent Activity (Raeq) reveals information regarding the degree of potential dangers from scattered radiation of crustal samples including concentrations from ^{40}K, ^{238}U and ^{232}Th. The Raeq in Becquerel per Kilogram (Bq kg^{-1}) for assessing activity concentrations was calculated using Equation 3.4 recommended by Beretka and Matthew (1985). On the premise that 10 Bq kg^{-1} of radium-226, 7 Bq kg^{-1} of thorium-232, and 130 Bq kg^{-1} of pottassium-40 provide equal gamma radiation dosage per unit time, Raeq was estimated using (UNSCEAR 1988);

$$Raeq\ (Bq\ kg^{-1}) = 0.077A_K + 1.43A_{Th} + A_U \quad (3.2)$$

3.5.4 Radioactive Heat Production

Equation 3.3, provided by Rybach (1988), was used to calculate the radioactive thermal energy production (A) per unit time. This is the quantity of thermal energy released per time by a sample of not too stable rock's

radioelement and associated isotopes in the process of disintegration. The nature and geochemical characteristics of the rocks in the area of study influence this component (Mareschal *et al.*, 2000; Maden and Akaryali 2015).

$$A\ (Wm^{-3}) = \rho\ (3.48\ eK + 2.56\ eTh + 9.52\ eU) \times 10^{-5} \qquad (3.3)$$

Where eK, eTh, and eU are the elemental concentrations of Pottassium-40 in weight (percentage), Uranium-238 and Thorium-232 in weight (part per million) respectively. The mean density of the sample is 2.70 gcc which implies 2700 kg m^{-3} (NGSA, 2009).

3.5.5 Outdoor and Indoor Annual Effective Dose

Assessment of human predisposition to radiation from airborne radiations and building materials referred to as outdoor annual effective dose and indoor annual effective dose in millisievert per year (mSv y^{-1}) indicated as AEDEout and AEDEin respectively, was determined using Equations 3.4 and 3.5 respectively. The outdoor occupancy value of 0.2 and indoor occupancy value of 0.8 was used according to UNSCEAR (2000). The conversion coefficient value (f) in sievert per gray per year (f = 0.7 × 10^{-6}Sv Gy^{-1}) for changing atmospheric absorbed dose (D_r) to annual effective dose, indoor and outdoor occupancy time value (T_o) for twelve months (24h × 365.25 ≅ 8760h) was used as values in Equation 3.6 (UNSCEAR, 2000) to get the Equations 3.6 and 3.7.

$$AEDEout\ (mSv\ y^{-1}) = D_r \times 0.7 \times 0.2 \times 8760 \times 10^{-6} \qquad (3.4)$$

$$AEDEin\ (mSv\ y^{-1}) = D_r \times 0.8 \times 8760 \times 0.7 \times 10^{-6} \qquad (3.5)$$

3.5.6 Internal and External Hazard Indices

In taking ^{222}Rn with its radioactive effect on humans to account, the external radioactive threat and internal radioactive threat indices connoted by RHex and RHin, respectively were estimated by applying Equations 3.6 and 3.7 (Ramasamy *et al.*, 2009).

$$RH_{ex} = A_K / 4810 + A_{Th} / 259 + A_U / 370 \qquad (3.6)$$

$$RH_{in} = A_K / 4810 + A_{Th} / 259 + A_U / 185 \qquad (3.7)$$

3.5.7 Gamma Representative Index

Using Equation 3.8 provided by the European Commission (EC) (1999), the Gamma Representative Indices (GRI) was applied to calculate the Gamma ray threat. This was linked with rock radioelement values that more than 1 milliSv y^{-1} indicates radiation threat.

$$AC = A_K / 3000 + A_{Th} / 200 + A_U / 300 \quad (3.8)$$

3.5.8 Activity Utilization Index

The computed activity utilization index (API) to establish the cumulative radiation hazard of ^{40}K, ^{238}U and ^{232}Th for the sample was done by applying Equation 3.9 (Ramasamy *et al.*, 2011).

$$API = (A_{Th} / 50\ Bq\ kg^{-1})f_{Th} + (A_u / 50\ Bq\ kg^{-1})f_u + (A_k / 500\ Bq\ kg^{-1})\ f_k \quad (3.9)$$

The components of the total dose rate at the factional level are f_K, f_{Th}, and f_U, which are related to gamma emission from the concentration of the real activities of the radioactive elements under study.

3.5.9. Annual Gonadal Effective Dose

Through research, it was discovered that gamma radiation exposure over safe levels can harm gonads and result in bone cancer (UNSCEAR, 1988). The yearly gonad effective dose (AGED) was estimated using Equation 3.10, given by Mamont-Ciesla *et al.* (1982).

$$AGDE\ (\mu Sv\ y^{-1}) = 0.314A_K + 3.09A_U + 4.18A_{Th} \quad (3.10)$$

3.5.10. Excessive Lifetime Cancer Risk

Gamma radiation exposure over acceptable levels can harm gonads and bone -marrow cancer in people (UNSCEAR, 1988), the beyond limit lifetime cancer threat (ELCR) was estimated according to Equation 3.11 (Taskin *et al.*, 2009)

$$ELCR = AEDE_{in} \times \xi \times F \quad (3.11)$$

F (0.05 Sv^{-1}) is the general population's cancer risk stochastic factor, and ξ is the lifetime expectancy of 60 years (Faweya & Adewumi, 2021; ICRP, 1990).

CHAPTER FOUR

4.0 RESULTS AND DISCUSSIONS

4.1 Elemental Concentration

The outcome of the estimated concentrations of potassium (^{40}K) in percentage (%) (eK), thorium (^{232}Th) and uranium (^{238}U) in parts per million (ppm) in Ilesha and environs basement rocks are presented in Table 4.1. The table shows the minimum values (min.), maximum values (max.), mean values (α) and mean deviations (δ) of the rocks' radionuclide concentration in distinct locations. The measured ^{40}K concentration have values from below detection limit (BDL) for Banded Gneiss (bG); north/east – south/west (NE-SW)) to 5.70% for Porphyritic Granite (OGp), (NE-SW); the concentration of thorium (eTh) ranged from BDL (bG, NE-SW; bG, E-W; GG, E-W) - 74.80 ppm (Quartzite (Qs), North-South (N-S)) while the concentration of uranium (eU) ranges from BDL – 22.50 ppm (Migmatite (M, NE-SW). The arithmetic mean (m) elemental concentrations of ^{40}K, ^{232}Th and ^{238}U for the rocks in various locations ranges from 0.30 (Undifferentiated schists, (Su), N-S) – 1.60% (OGp, N-S; Bg, East – West (E-W); 2.80 (M, NE-SW) – 17.00 ppm (Qs, N-S) and 0.70 (M, NE-SW) – 4.70 ppm (Qs, N-S) respectively.

The spatial distributions generated for the rocks' radionuclides in various locations of the area of study with the detector are shown as Fig. 4.1 – 4.3. In Fig. 4.1, a large part of the north of the study area shows a very large ^{40}K concentration with values from 1.66% to greater than 5.70%. Rocks located in the centre shows intermediate to low ^{40}K concentration with values from BDL–1.26%. In Fig. 4.2, rocks in the south to west location in the area show a low to slightly high ^{232}Th (BDL–74.80 ppm). ^{232}Th concentration with high values from 6.04 to 74.80 ppm characterised the rocks around the north-east axis and this suggests very rich ^{232}Th bearing mineral in the area of study.

In Fig. 4.3, low ^{232}U concentration was noticed in rocks in the location N-W and S-W with concentration majorly between BDL to 2.54 ppm. The Rocks around

the N-E and the south reveals high eU between 2.93 – 22.50 ppm.

Table 4.1 Distribution of Elemental Concentration of Ilesha and Environs Basement Complex Rocks at various Locations. The table shows the minimum (Min.), maximum (Max.), means (α) and deviation values (α)

Profile	Rock Type	Elemental concentration											
		K%				^{232}Th(ppm)				^{238}U (ppm)			
		Min.	Max.	α	δ	Min.	Max.	α	δ	Min.	Max	α	δ
N-S	bG	0.10	3.20	0.80	0.50	0.10	41.70	9.40	7.70	0.80	8.70	3.20	1.60
	bG	0.10	3.60	1.00	1.00	1.90	16.20	8.90	3.00	BDL	5.40	2.30	1.40
	bG	0.10	4.70	1.30	1.20	2.90	23.70	10.50	3.80	0.40	6.40	2.60	1.10
	M	0.10	1.90	0.70	0.30	1.00	27.70	9.10	5.10	BDL	9.90	2.30	1.70
	M	0.10	2.90	0.70	0.50	1.50	44.50	10.10	7.40	BDL	15.80	2.60	2.70
	OGp	0.30	4.10	1.30	1.20	3.00	31.90	11.50	5.50	BDL	8.80	2.70	1.40
	OGp	0.10	4.30	1.60	1.20	4.30	37.10	14.50	6.80	0.40	7.70	3.40	1.60
	Qs	0.10	4.60	1.30	1.30	4.80	39.50	17.00	8.40	0.30	11.70	4.70	2.50
	Qs	0.10	2.80	0.70	0.60	3.00	74.80	15.80	11.50	BDL	11.80	3.40	1.70
	Qs	0.10	1.70	0.70	0.40	3.90	39.90	15.20	7.00	BDL	9.50	3.50	2.00
	Qs	0.10	1.50	0.40	0.20	2.20	26.50	8.20	4.90	BDL	7.30	1.80	1.50
	Qs	0.10	2.60	0.70	0.40	2.10	20.40	8.30	3.30	BDL	7.00	2.70	1.40
	Su	0.20	3.70	0.90	0.60	1.50	19.00	8.10	4.00	0.90	7.80	3.40	1.10
	Su	BDL	1.00	0.30	0.20	0.20	25.10	7.20	4.60	BDL	6.90	1.80	1.00
	Su	0.10	1.30	0.30	0.20	1.30	22.50	8.20	4.20	0.10	6.70	2.20	1.10
NE-SW	bG	0.30	2.80	1.20	0.60	BDL	20.30	8.20	3.90	BDL	5.60	3.20	1.10
	bG	0.10	3.90	1.40	1.20	0.40	16.30	7.90	3.30	0.70	6.70	2.80	1.10
	bG	0.10	4.60	1.20	1.10	2.90	28.90	9.80	4.40	0.40	7.30	3.00	1.10
	bG	0.00	3.70	1.20	1.00	1.70	31.50	10.90	4.60	BDL	7.20	2.80	1.10
	bG	BDL	4.80	1.30	1.10	0.00	44.10	11.80	6.40	0.60	6.90	3.00	1.00
	bG	0.10	4.20	1.00	1.00	0.40	38.70	11.60	6.10	0.30	9.40	2.80	1.50
	M	0.30	0.90	0.70	0.10	3.00	13.20	6.30	2.90	1.00	3.50	2.30	0.70

	M	0.20	1.90	0.80	0.50	3.20	16.30	9.40	2.80	1.10	4.10	2.50	0.70
	M	0.00	2.00	0.50	0.40	1.00	27.20	2.80	5.70	BDL	9.50	2.10	1.80
	M	0.10	3.50	0.80	0.60	2.00	43.60	10.20	9.40	BDL	22.50	3.60	4.30
	M	0.00	2.10	0.60	0.40	1.10	25.80	6.50	2.90	BDL	7.00	1.60	1.50
	M	0.00	1.40	0.70	0.30	2.90	20.10	8.20	4.00	BDL	6.60	1.90	1.60
	M	0.00	1.40	0.60	0.40	1.20	10.90	5.90	2.20	BDL	4.50	0.70	1.20
	OGp	0.10	5.70	1.20	1.30	4.50	39.40	16.80	8.00	BDL	11.20	4.30	2.20
	OGp	0.10	1.60	0.60	0.40	2.80	29.70	13.30	3.90	0.20	6.60	3.10	1.10
	OGp	0.10	1.50	0.50	0.20	4.70	23.40	12.30	3.80	0.60	6.50	2.90	1.00
	Qs	0.00	2.60	0.70	0.40	2.10	20.40	8.30	3.30	BDL	7.00	2.70	1.40
	Qs	0.00	1.40	0.50	0.30	1.70	20.20	9.30	3.90	BDL	1.50	2.80	1.80
	Qs	0.00	2.30	0.60	0.40	0.80	51.00	11.00	10.30	BDL	12.80	2.70	2.60
	Qs	0.00	2.10	0.60	0.40	1.70	34.60	10.00	7.30	BDL	8.20	2.40	1.70
	Qs	0.00	2.20	0.60	0.50	0.00	19.80	7.60	4.00	BDL	7.10	1.50	1.40
	Su	0.20	1.90	0.60	0.30	0.50	41.80	11.20	7.00	0.30	8.80	3.30	1.50
	Su	0.20	2.90	0.70	0.50	1.20	53.70	9.60	8.30	0.60	9.90	3.30	1.40
	Su	BDL	4.60	1.20	1.10	1.60	27.00	9.40	5.30	0.40	7.60	3.10	1.40
	Su	0.10	4.00	1.30	1.10	1.00	22.70	9.10	4.70	0.50	7.60	3.20	1.40
E-W	bG	0.10	4.60	1.60	1.20	BDL	31.90	10.00	6.00	BDL	9.10	2.80	1.70
	bG	0.20	4.10	1.50	1.20	BDL	30.30	10.50	5.20	BDL	12.50	3.20	1.90
	bG	0.10	4.20	1.30	1.10	0.40	32.70	11.30	7.60	0.30	10.70	3.60	2.00
	bG	0.00	4.00	1.00	1.00	1.50	43.00	12.00	8.40	BDL	10.80	3.60	2.20
	bG	0.10	2.00	0.50	0.30	0.90	25.80	8.90	5.30	BDL	8.50	2.60	1.40
	bG	0.00	1.90	0.50	0.30	0.20	29.40	8.40	5.30	BDL	8.80	2.50	1.40
	Ch	0.10	3.20	0.80	0.60	0.40	32.00	10.30	6.40	BDL	6.90	2.50	1.50
	Ch	0.10	2.80	0.70	0.50	1.90	53.30	10.60	6.80	BDL	7.50	2.50	1.60
	GG	0.00	4.10	1.20	1.10	1.60	25.40	12.10	5.10	0.30	9.10	2.80	1.30
	GG	0.10	4.10	1.20	1.10	1.20	25.70	11.00	5.00	0.40	6.30	2.70	1.10
	GG	0.10	4.30	1.30	1.00	BDL	27.20	11.10	4.90	BDL	6.30	2.70	1.10
	Su	0.00	3.00	0.6	0.5	1.50	42.7	11.0	7.10	BDL	7.70	2.80	1.60

			0	0		0	0					
Su	0.00	2.40	0.40	0.30	2.40	44.20	10.30	5.90	0.00	11.90	2.70	1.50
Su	0.10	2.70	0.50	0.40	2.40	25.20	9.00	4.10	BDL	6.50	2.40	1.50
Su	0.10	2.00	0.50	0.30	1.50	25.30	8.30	4.60	BDL	6.70	2.20	1.40
Su	0.00	2.90	0.60	0.50	0.10	46.50	9.30	6.60	BDL	8.60	2.40	1.70
Su	0.10	2.90	0.60	0.50	1.10	45.30	11.50	7.70	BDL	8.60	2.60	1.80
Su	0.10	3.80	0.80	0.70	1.00	26.90	10.80	5.30	BDL	9.00	2.60	1.60
Su	0.10	4.00	1.00	0.90	1.40	38.00	11.60	7.00	BDL	7.80	2.90	1.90
Su	0.00	3.00	0.80	0.50	0.90	38.40	11.00	6.70	BDL	7.60	2.90	1.90

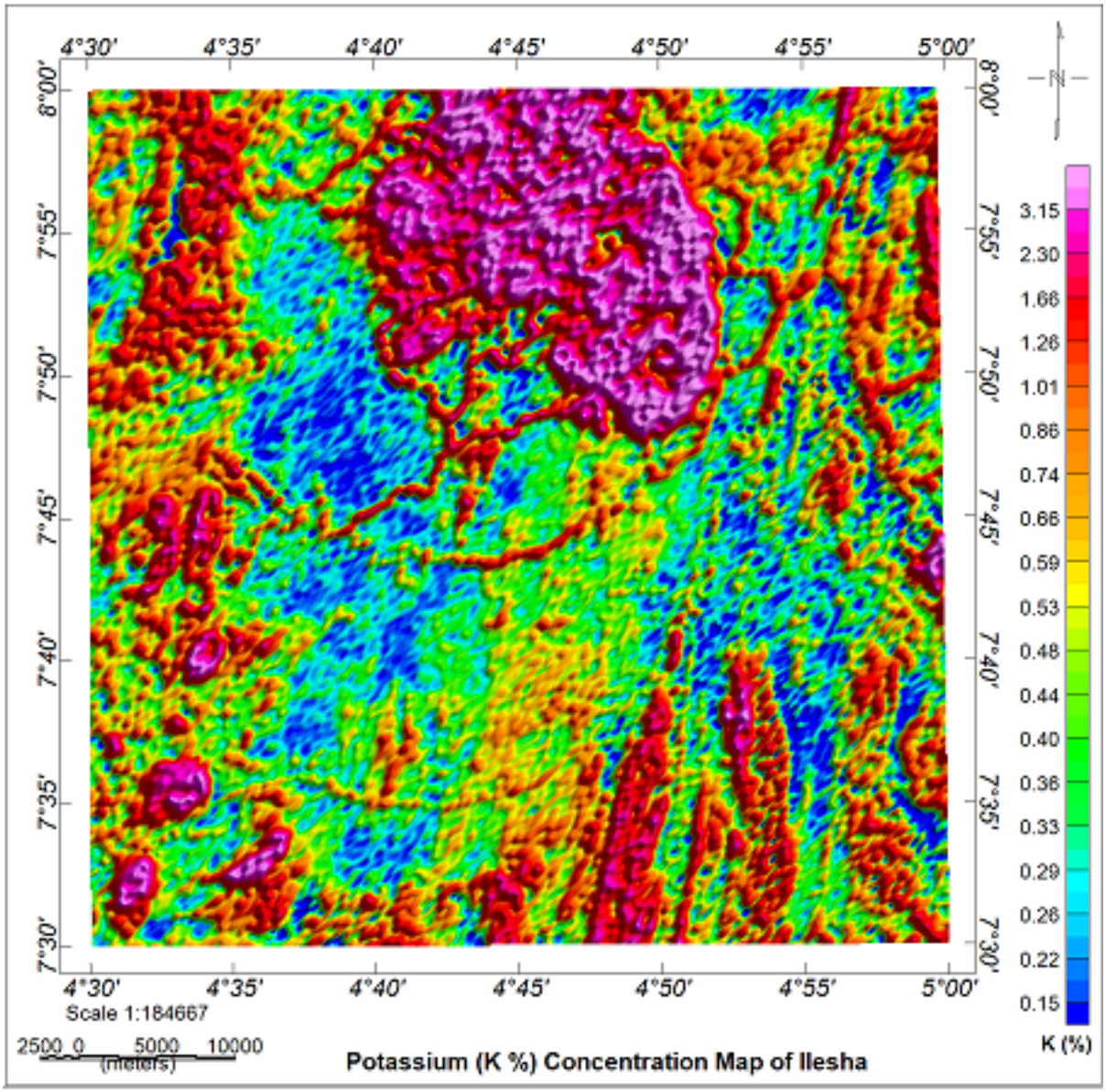

Figure 4.1: Map of Potassium Concentration of Ilesha and Environs Basement

Complex Rocks

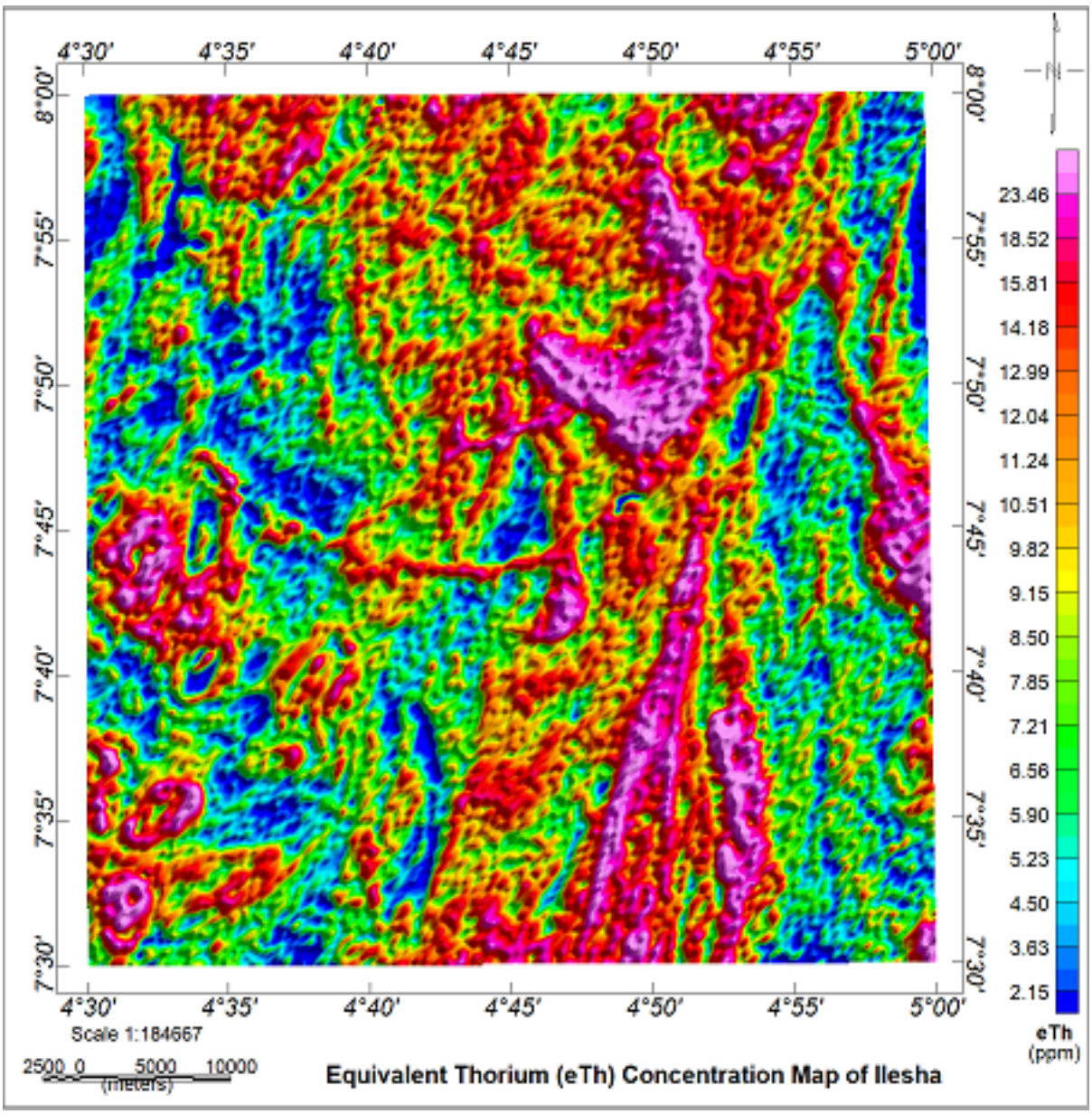

Figure 4.2: Map of Thorium Concentration of Ilesha and Environs Basement Complex Rocks

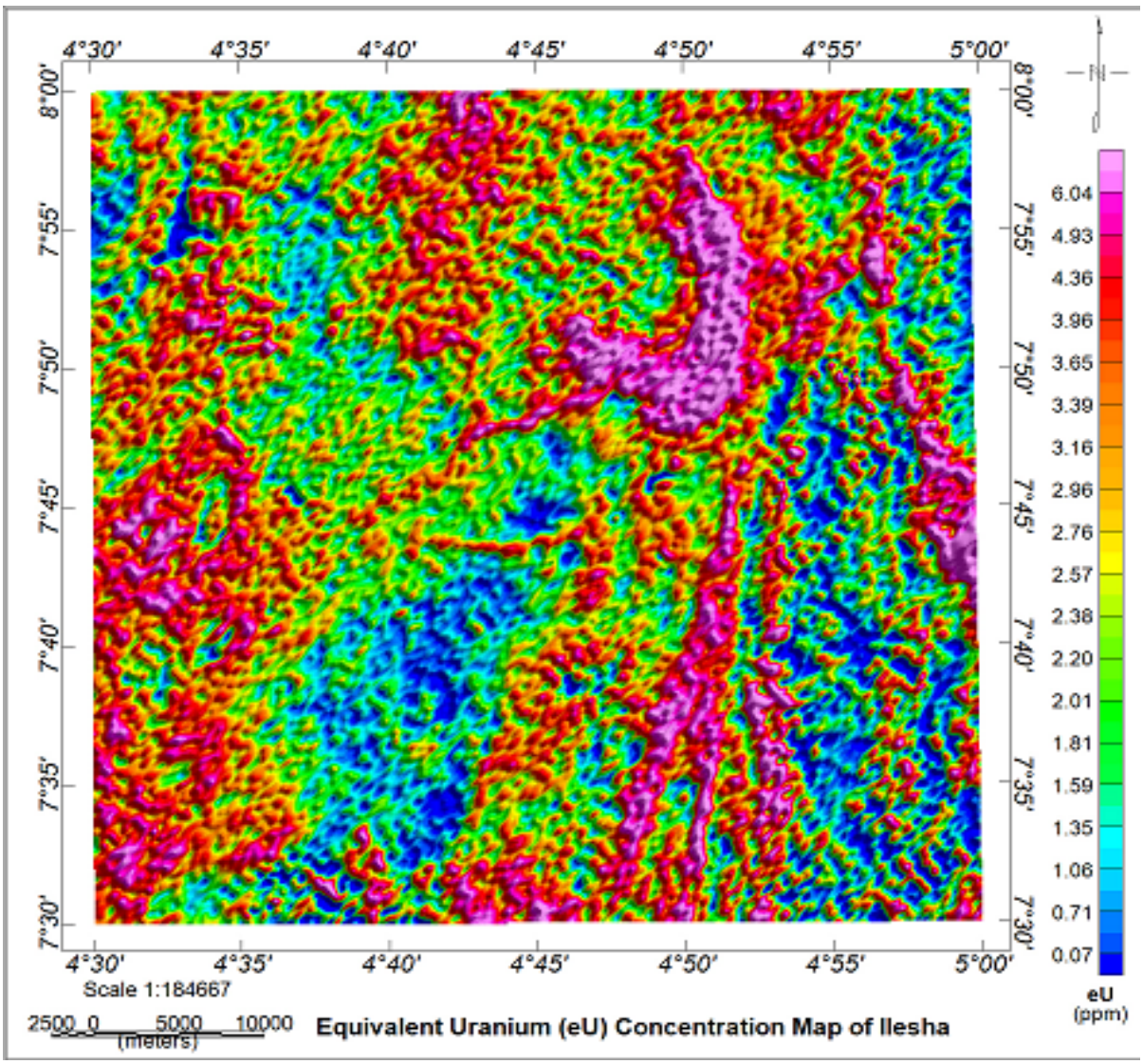

Figure 4.3: Map of Uranium Concentration of Ilesha and Environs Basement Complex Rocks

4.2 Activity Concentration

The estimated average radioelement concentration and activity concentrations of thorium, potassium and uranium of each rock are presented in Table 4.2. The Table gives the measured values of these radionuclides in various rocks and their overall mean values in Bq kg^{-1} was given to estimate the levels of their concentration and compare their mean values with the global mean values. The estimated activity concentrations for ^{40}K, ^{232}Th and ^{238}U for various rocks in different locations are as high as 500.80 Bq kg^{-1} (OGp, N-S; bG, E-W), 69.02 Bq kg^{-1} (Qs, N-S) and 58.75 Bq kg^{-1} (Qs, N-S) respectively. Their average activity concentrations ranged from 93.90 –500.80, 11.37 – 69.02 and 18.75 – 58.75 Bq kg^{-1} for potassium, thorium and uranium, respectively. Estimated overall mean value of 0.85% estimated for elemental concentrations of ^{40}K, is below the average crustal concentrations of 2.35%, the overall mean value of 2.76 ppm estimated for elemental concentrations of ^{238}U is below the average crustal concentrations of 3 ppm and the overall mean value of 10.13 ppm estimated for elemental concentrations of ^{232}Th is below the average crustal concentrations of 12 ppm (IAEA, 2003).

The mean activity concentrations values of 267.09 and 41.17 Bq kg^{-1} for ^{40}K and ^{232}Th are below the crustal values of 420.00 and 45.00 Bq kg^{-1} respectively while the environmental activity concentrations of 34.40 for ^{238}U is above the crustal standards of 33 Bq kg^{-1} (UNSCEAR, 2000).

4.3 Dose Assessment

Results of the estimated dose per unit time (D_r) in various locations are presented in the Table 4.2. The values range from 25.71 (bG, NE-SW) to 86.97 $nGyh^{-1}$ (Qs, N-S). The estimated overall mean absorbed dose rate for the rocks is 52.60 $nGyh^{-1}$ (Table 4.2). This value is below the global average but fits in the safety range of 28 – 120 nGy h^{-1} according to UNSCEAR (2000).

Table 4.2 Dose Assessment for the Rocks of Ilesha and environs for various Locations

Profile	Rock type	K%	eTh (ppm)	eU (ppm)	A_K (Bq kg^{-1})	A_{Th} (Bq Kg^{-1})	A_U (Bq Kg^{-1})	D_r (nGy h^{-1})
N-S	bG	0.80	9.40	3.20	250.40	38.16	40.00	52.62
		1.00	8.90	2.30	313.00	36.13	28.75	48.77
		1.30	10.50	2.60	406.90	42.63	32.50	58.46
	M	0.70	9.10	2.30	219.10	36.95	28.75	45.36
		0.70	10.10	2.60	219.10	41.01	32.50	49.62
	OGp	1.30	11.50	2.70	406.90	46.69	33.75	61.55
		1.60	14.50	3.40	500.80	58.87	42.50	77.08
	Qs	1.30	17.00	4.70	406.90	69.02	58.75	86.97
		0.70	15.80	3.40	219.10	64.15	42.50	68.61
		0.70	15.20	3.50	219.10	61.71	43.75	67.67
		0.40	8.20	1.80	125.20	33.29	22.50	36.29
		0.70	8.30	2.70	219.10	33.70	33.75	45.66
	Su	0.90	8.10	3.40	281.70	32.89	42.50	51.80
		0.30	7.20	1.80	93.90	29.23	22.50	32.46
		0.30	8.20	2.20	93.90	33.29	27.50	37.29
NE-SW	bG	1.20	8.20	3.20	375.60	33.29	40.00	54.82
		1.40	7.90	2.80	438.20	32.07	35.00	54.36
		1.20	9.80	3.00	375.60	39.79	37.50	57.70
		1.20	10.90	2.80	375.60	44.25	35.00	59.31
		1.30	11.80	3.00	406.90	47.91	37.50	64.04
		1.00	11.60	2.80	313.00	47.10	35.00	58.47
	M	0.70	6.30	2.30	219.10	25.58	28.75	38.30
		0.80	9.40	2.50	250.40	38.16	31.25	48.58
		0.50	2.80	2.10	156.50	11.37	26.25	25.71
		0.80	10.20	3.60	250.40	41.41	45.00	56.95
		0.60	6.50	1.60	187.80	26.39	20.00	33.46
		0.70	8.20	1.90	219.10	33.29	23.75	40.78
		0.60	5.90	0.70	187.80	23.95	8.75	26.75
	OGp	1.20	16.80	4.30	375.60	68.21	53.75	82.85
		0.60	13.30	3.10	187.80	54.00	38.75	59.27
		0.50	12.30	2.90	156.50	49.94	36.25	54.29
	Qs	0.70	8.30	2.70	219.10	33.70	33.75	45.66
		0.50	9.30	2.80	156.50	37.76	35.00	46.14
		0.60	11.00	2.70	187.80	44.66	33.75	51.16
		0.60	10.00	2.40	187.80	40.60	30.00	46.90
		0.60	7.60	1.50	187.80	30.86	18.75	35.66
	Su	0.60	11.20	3.30	187.80	45.47	41.25	55.13

		0.70	9.60	3.30	219.10	38.98	41.25	52.40
		1.20	9.40	3.10	375.60	38.16	38.75	57.26
		1.30	9.10	3.20	406.90	36.95	40.00	58.39
E-W	bG	1.60	10.00	2.80	500.80	40.60	35.00	62.27
		1.50	10.50	3.20	469.50	42.63	40.00	64.53
		1.30	11.30	3.60	406.90	45.88	45.00	66.25
		1.00	12.00	3.60	313.00	48.72	45.00	64.10
		0.50	8.90	2.60	156.50	36.13	32.50	43.98
		0.50	8.40	2.50	156.50	34.10	31.25	42.14
	Ch	0.80	10.30	2.50	250.40	41.82	31.25	50.85
		0.70	10.60	2.50	219.10	43.04	31.25	50.30
	GG	1.20	12.10	2.80	375.60	49.13	35.00	62.34
		1.20	11.00	2.70	375.60	44.66	33.75	58.99
		1.30	11.10	2.70	406.90	45.07	33.75	60.55
	Su	0.60	11.00	2.80	187.80	44.66	35.00	51.74
		0.40	10.30	2.70	125.20	41.82	33.75	46.78
		0.50	9.00	2.40	156.50	36.54	30.00	43.08
		0.50	8.30	2.20	156.50	33.70	27.50	40.16
		0.60	9.30	2.40	187.80	37.76	30.00	45.14
		0.60	11.50	2.60	187.80	46.69	32.50	51.84
		0.80	10.80	2.60	250.40	43.85	32.50	52.69
		1.00	11.60	2.90	313.00	47.10	36.25	59.05
		0.80	11.00	2.90	250.40	44.66	36.25	54.92

4.4 Total Count Emission Rate

The Total Count Emission rate (TC) map (Fig. 4.4), reveals total emission per unit time from the three radioelements. Large continuous radioactive release of values greater than two hundred counts per unit time (cps) was noticed in the north axis, north-western and east to south-eastern locations of the area. This indicates large presence of naturally occurring radionuclide materials (NORMs). The other locations reveal low to medium emission per unit time, from 780.34 to 2000.00 cps for these radioelements.

The estimated total count emission per unit time for the rocks and mean values are presented in table 4.3. Migmatite (M) within the north-east to south -west emits the smallest activity rate of 780.34 cps and the quartzite within the north-south emits the greatest with 2639.97 cps combined radioactivity. TC mean for the samples have values from 25.45 nGy h^{-1} (M around N-E to S-W) and 86.09 nGy h^{-1} (Qs, around N-S) with mean value of 1597.20 cps.

Table 4.3: Distribution of Total Counts Emission Rate of rocks of Ilesha and

Environs at various Locations

Profile	Rock type	K%	eTh (ppm)	eU (ppm)	Tc (nGy h^{-1})
N-S	bG	0.80	9.40	3.20	52.08
		1.00	8.90	2.30	48.33
		1.30	10.50	2.60	57.95
	M	0.70	9.10	2.30	44.91
		0.70	10.10	2.60	49.11
	OGp	1.30	11.50	2.70	61.01
		1.60	14.50	3.40	76.39
	Qs	1.30	17.00	4.70	86.09
		0.70	15.80	3.40	67.87
		0.70	15.20	3.50	66.94
		0.40	8.20	1.80	35.90
		0.70	8.30	2.70	45.19
	Su	0.90	8.10	3.40	51.28
		0.30	7.20	1.80	32.10
		0.30	8.20	2.20	36.87
NE-SW	bG	1.20	8.20	3.20	54.31
		1.40	7.90	2.80	53.91
		1.20	9.80	3.00	57.17
		1.20	10.90	2.80	58.78
		1.30	11.80	3.00	63.46
		1.00	11.60	2.80	57.91
	M	0.70	6.30	2.30	37.93
		0.80	9.40	2.50	48.10
		0.50	2.80	2.10	25.45
		0.80	10.20	3.60	56.34
		0.60	6.50	1.60	33.14
		0.70	8.20	1.90	40.39
		0.60	5.90	0.70	26.54
	OGp	1.20	16.80	4.30	82.01
		0.60	13.30	3.10	58.62
		0.50	12.30	2.90	53.68
	Qs	0.70	8.30	2.70	45.19
		0.50	9.30	2.80	45.63
		0.60	11.00	2.70	50.61
		0.60	10.00	2.40	46.41
		0.60	7.60	1.50	35.32
	Su	0.60	11.20	3.30	54.52
		0.70	9.60	3.30	51.83
		1.20	9.40	3.10	56.74
		1.30	9.10	3.20	57.87
E-W	bG	1.60	10.00	2.80	61.76

	1.50	10.50	3.20	63.97
	1.30	11.30	3.60	65.62
	1.00	12.00	3.60	63.45
	0.50	8.90	2.60	43.50
	0.50	8.40	2.50	41.68
Ch	0.80	10.30	2.50	50.35
	0.70	10.60	2.50	49.79
GG	1.20	12.10	2.80	61.77
	1.20	11.00	2.70	58.46
	1.30	11.10	2.70	60.02
Su	0.60	11.00	2.80	51.18
	0.40	10.30	2.70	46.25
	0.50	9.00	2.40	42.61
	0.50	8.30	2.20	39.73
	0.60	9.30	2.40	44.67
	0.60	11.50	2.60	51.29
	0.80	10.80	2.60	52.16
	1.00	11.60	2.90	58.47
	0.80	11.00	2.90	54.36

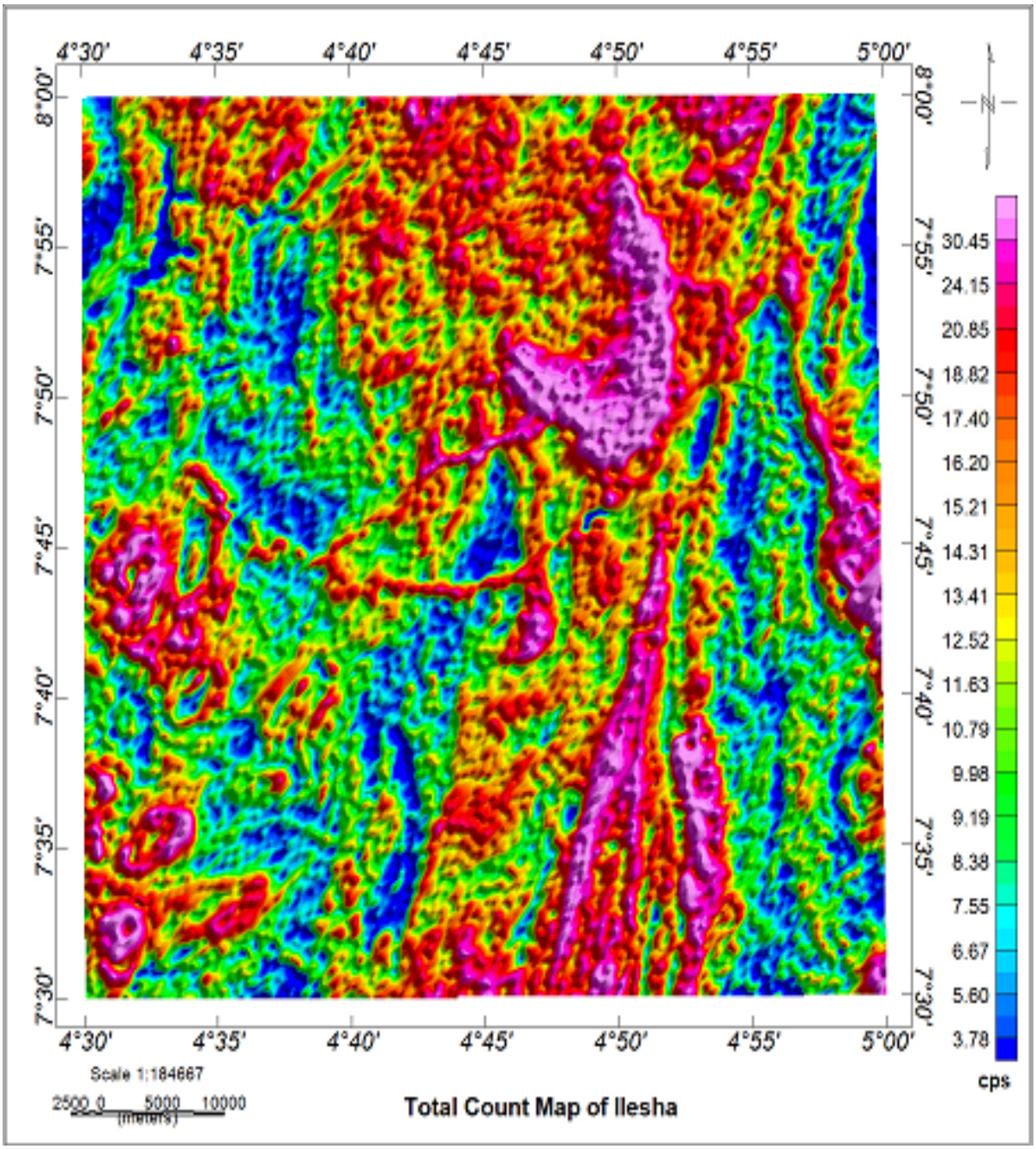

Figure 4.4: Map of Count Emission per unit time of rocks of Ilesha and Environs

4.5. Radium Equivalent Activity

The Radium Equivalent (Raeq) activity of rocks of Ilesha and environs reveals knowledge about risks of radiation coming out of crustal rocks of ^{40}K, ^{238}U and ^{232}Th compositions. The evaluated mean Raeq for the rocks are presented in the Table 4.4. The results have values from 54.56 (M, NE-SW) to 188.78 Bq kg^{-1} (Qs, N-S) with overall mean of 113.85 Bq kg^{-1}. This measured average is not up to the global average of 370 Bq kg^{-1} according to UNSCEAR (2000); indicating a non-threat posing value.

4.6 Radioactive Heat Production

According to Table 4.4, the obtained averages of radioactive heat production (A) for the rocks in various locations have value from 0.64 (M, NE-SW) to 2.49 μWm^{-3} (Qs, N-S) with total average of 1.48 $\mu W\ m^{-3}$ (see Table 4.6). The A mean (1.48 μWm^{-3}) is more than the crustal mean permissible range of 0.8–1.2 μWm^{-3} (Bea 2012; Youssef 2016); suggesting notable addition to thermal energy flux of the area.

4.7 Outdoor and Indoor Annual Effective Dose

The results of AEDEout and AEDEin, estimated for the rocks of Ilesha and environs is to check if the location is radiological safe for dwellers or not (Table 4.6). The AEDEout for the location have values from 0.03 to 0.11 $mSvy^{-1}$ while that for AEDEin range from 0.13 to 0.43 $mSvy^{-1}$, having average values of 0.06 and 0.26 mSv y^{-1} respectively. The estimated averages; 0.06 $mSvy^{-1}$ and 0.26 $mSvy^{-1}$ for AEDE for outdoor and indoor are below the mean worldwide values of 0.07 mSv $y^{-1}$and 0.41 mSv y^{-1} respectively. OGp (0.38 $mSvy^{-1}$) and Qs (0.43 $mSvy^{-1}$) in the N-S have values above this world average values according to UNSCEAR (2000). The measured averages are not up to the world upper permit of 1 mSv y^{-1} according to ICRP (1977).

Table 4.4: Radium Equilibrium, Radioactive Heat Production (A), Annual Effective Dose (AEDE) for the Rocks of Ilesha and Environs at various locations

Profile	Rock Type	Ra_{eq} (Bq kg^{-1})	A(μW m^{-3})	D(nGy h^{-1})	AEDEout (mSv y^{-1})	AEDEin (mSv y^{-1})
N-S	bG	113.86	1.54	52.62	0.06	0.26
		104.52	1.29	48.77	0.06	0.24
		124.79	1.50	58.46	0.07	0.29
	M	98.45	1.28	45.36	0.06	0.22
		108.01	1.42	49.62	0.06	0.24
	OGp	131.85	1.60	61.55	0.08	0.30
		165.25	2.01	77.08	0.09	0.38
	Qs	188.78	2.49	86.97	0.11	0.43
		151.10	2.02	68.61	0.08	0.34
		148.87	2.00	67.67	0.08	0.33
		79.75	1.06	36.29	0.04	0.18
		98.81	1.32	45.66	0.06	0.22
	Su	111.22	1.51	51.80	0.06	0.25
		71.53	0.98	32.46	0.04	0.16
		82.34	1.15	37.29	0.05	0.18
NE-SW	bG	116.53	1.49	54.82	0.07	0.27
		114.61	1.39	54.36	0.07	0.27
		123.32	1.55	57.70	0.07	0.28
		127.20	1.57	59.31	0.07	0.29
		137.34	1.70	64.04	0.08	0.31
		126.45	1.60	58.47	0.07	0.29
	M	82.20	1.08	38.30	0.05	0.19
		105.11	1.36	48.58	0.06	0.24
		54.56	0.77	25.71	0.03	0.13
		123.50	1.69	56.95	0.07	0.28
		72.20	0.91	33.46	0.04	0.16
		88.23	1.11	40.78	0.05	0.20
		57.46	0.64	26.75	0.03	0.13
	OGp	180.21	2.36	82.85	0.10	0.41
		130.43	1.76	59.27	0.07	0.29
		119.71	1.63	54.29	0.07	0.27
	Qs	98.81	1.32	45.66	0.06	0.22
		101.04	1.40	46.14	0.06	0.23
		112.07	1.50	51.16	0.06	0.25
		102.52	1.35	46.90	0.06	0.23
		77.33	0.96	35.66	0.04	0.17
	Su	120.74	1.67	55.13	0.07	0.27
		113.86	1.57	52.40	0.06	0.26

		122.25	1.55	57.26	0.07	0.28
		124.16	1.56	58.39	0.07	0.29
E-W	bG	131.62	1.55	62.27	0.08	0.31
		137.11	1.68	64.53	0.08	0.32
		141.94	1.82	66.25	0.08	0.32
		138.77	1.84	64.10	0.08	0.31
		96.22	1.32	43.98	0.05	0.22
		92.07	1.26	42.14	0.05	0.21
	Ch	110.33	1.42	50.85	0.06	0.25
		109.66	1.43	50.30	0.06	0.25
	GG	134.17	1.66	62.34	0.08	0.31
		126.54	1.56	58.99	0.07	0.29
		129.53	1.57	60.55	0.07	0.30
	Su	113.32	1.53	51.74	0.06	0.25
		103.19	1.43	46.78	0.06	0.23
		94.30	1.28	43.08	0.05	0.21
		87.74	1.18	40.16	0.05	0.20
		98.45	1.31	45.14	0.06	0.22
		113.73	1.51	51.84	0.06	0.25
		114.48	1.48	52.69	0.06	0.26
		127.70	1.63	59.05	0.07	0.29
		119.39	1.57	54.92	0.07	0.27

4.8 Internal and External Hazard Indices

External and Internal hazard Indices are presented in Table 4.6. The External hazard Index (RHex) ranges from 0.15 (M, NE-SW) to 0.51 (Qs, N-S) with average of 0.31. The Internal hazard Index (RHin) have values from 0.18 (M, NE-SW) to 0.67(Qs, N-S) with mean value of 0.40. These values are not up to the permissible limit of 1 according to Ramasamy *et al.* (2009).

4.9 Gamma Representative Index

The gamma representative index (AC) was estimated and presented in Table 4.6. It is the measure of the effects of gamma radiations on humans. Its values are from 0.20 to 0.68 with average of 0.41. This figure, which is less than 2 (AC ≤ 2), correspond to gamma activity that have no threat to occupants OF Ilesha and environs's health (EC, 1999).

4.10. Activity Utilization Index

The activity utilization index (API) for estimating threats connected to gamma ray doses from radioelements of ^{40}K, ^{232}Th and ^{238}U in the rocks are presented in the Table 4.6. These values ranges from 0.39 (M, NE-SW) to 1.41 (Qs, N-S) with mean value 0.84 (API < 2) is of lower value compared with 0.3 mSv y^{-1} according to El-Gamal *et al.*, (2007). Moreover, the two values suggest that the gamma radiation effect is negligible.

4.11. Annual Gonadal Effective Dose

According to Table 4.6, the estimated annual gonadal effective dose (AGED) values ranged from 177.77 (M, NE-SW) to 597.81μSvy^{-1} (Qs, N-S) with an average value of 362.30 μSvy^{-1} (Table 4.7). These estimates have values that are more than the globe permit of 300 μSv y^{-1} for AGED according to Xinwei *et al.*, (2006).

An AGED value more than the global permits may necessarily not indicate health threat to the gonad of Ilesha and environs residents. However, it could suggest that people should reduce usage of rocks having radionuclides

concentration that is more than the permissible limit.

Table 4.6: External and Internal Hazard Indices, Gamma Representative, Activity Utilization Index, Annual Gonadal Effective Dose, Excessive Lifetime Cancer Risk for the Rocks of Ilesha and Environs at various locations

Profile	Rock Type	RHex	RHin	AC	AUI	AGDE ($\mu Sv\ y^{-1}$)	ELCR
N-S	bG	0.31	0.42	0.41	0.85	361.75	0.90
		0.28	0.36	0.38	0.73	338.16	0.84
		0.34	0.42	0.46	0.85	406.39	1.00
	M	0.27	0.34	0.35	0.73	312.07	0.78
		0.29	0.38	0.39	0.81	340.63	0.85
	OGp	0.36	0.45	0.48	0.91	427.22	1.06
		0.45	0.56	0.60	1.14	534.65	1.32
	Qs	0.51	0.67	0.68	1.41	597.81	1.49
		0.41	0.52	0.54	1.19	468.26	1.18
		0.40	0.52	0.53	1.17	461.94	1.16
		0.22	0.28	0.28	0.62	248.00	0.62
		0.27	0.36	0.35	0.74	313.94	0.78
	Su	0.30	0.42	0.40	0.81	357.24	0.89
		0.19	0.25	0.25	0.57	221.20	0.56
		0.22	0.30	0.29	0.66	253.62	0.64
NE-SW	bG	0.31	0.42	0.42	0.80	380.70	0.94
		0.31	0.40	0.42	0.75	379.81	0.93
		0.33	0.43	0.45	0.86	400.13	0.99
		0.34	0.44	0.46	0.89	411.07	1.02
		0.37	0.47	0.50	0.96	443.90	1.10
		0.34	0.44	0.46	0.92	403.29	1.00
	M	0.22	0.30	0.30	0.59	264.55	0.66
		0.28	0.37	0.38	0.77	334.71	0.83
		0.15	0.22	0.20	0.39	177.77	0.44
		0.33	0.46	0.44	0.94	390.78	0.98
		0.19	0.25	0.26	0.52	231.08	0.57
		0.24	0.30	0.32	0.64	281.35	0.70
		0.16	0.18	0.21	0.39	186.13	0.46
	OGp	0.49	0.63	0.65	1.35	569.14	1.42
		0.35	0.46	0.46	1.03	404.42	1.02
		0.32	0.42	0.42	0.95	369.89	0.93
	Qs	0.27	0.36	0.35	0.74	313.94	0.78
		0.27	0.37	0.36	0.79	315.12	0.79
		0.30	0.39	0.40	0.87	349.94	0.88
		0.28	0.36	0.37	0.78	321.38	0.81

		0.21	0.26	0.28	0.56	245.88	0.61
	Su	0.33	0.44	0.43	0.95	376.50	0.95
		0.31	0.42	0.41	0.87	359.18	0.90
		0.33	0.43	0.45	0.85	397.20	0.98
		0.34	0.44	0.45	0.85	405.80	1.00
E-W	bG	0.36	0.45	0.49	0.85	435.11	1.07
		0.37	0.48	0.50	0.92	449.22	1.11
		0.38	0.50	0.52	1.00	458.59	1.14
		0.37	0.50	0.50	1.03	440.98	1.10
		0.26	0.35	0.34	0.75	300.61	0.76
		0.25	0.33	0.33	0.71	288.26	0.72
	Ch	0.30	0.38	0.40	0.81	349.99	0.87
		0.30	0.38	0.39	0.83	345.25	0.86
	GG	0.36	0.46	0.49	0.95	431.44	1.07
		0.34	0.43	0.46	0.88	408.90	1.01
		0.35	0.44	0.47	0.89	420.43	1.04
	Su	0.31	0.40	0.40	0.88	353.80	0.89
		0.28	0.37	0.36	0.83	318.40	0.80
		0.25	0.34	0.33	0.73	294.58	0.74
		0.24	0.31	0.31	0.67	274.97	0.69
		0.27	0.35	0.35	0.75	309.50	0.78
		0.31	0.39	0.40	0.88	354.56	0.89
		0.31	0.40	0.41	0.85	362.34	0.90
		0.34	0.44	0.46	0.93	407.16	1.01
		0.32	0.42	0.43	0.89	377.32	0.94

4.12. Excessive Lifetime Cancer Risk

The estimated values for the excessive lifetime cancer threat (ELCR) range from 4.40×10^{-4} to 1.49×10^{-3}, having an average of 9.00×10^{-3} (Table 4.10). The estimated figures are large compared with the global permits of 2.90×10^{-4} ELCR (Tufail *et al*., 2007). This higher value suggests caution in the use of rocks with high radionuclides concentration from the study area.

4.13 Comparison of Airborne Radioactive Survey of Ilesha and Environs with Mean values in various locations of the globe

According to Table 4.7, this work favourably compares with other radiological indices in various locations of the globe.

Table 4.7: Comparison of Airborne Radioactive Survey of Ilesha and Environs with Mean values in various locations of the globe

	Activity concentration ($BqKg^{-1}$)			D ($nGyh^{-1}$)	$AEDE_{in}$ ($mSvy^{-1}$)	ELCR (10^{-3})	References
	^{40}K	^{232}Th	^{238}U				
China	580.00	49.00	40.00				Tan *et al*. (1991)
Hong Kong	530.00	95.00	59.00	87.00			UNSCEAR (2000);
Malaysia				92.00		2.50	UNSCEAR (2000)
Pakistan				70.00	0.49	0.54	Rafique *et al*. (2014)
Mulga city, Turkey	340.00	27.00	28.50	53.00			Erbek and Dolmaz (2018)
Tamilnadu, India	1146.88	48.56	19.16	40-135		0.70	Chandrasekaran *et al*. (2014)
United states	370.00	35.00	40.00	47.00			UNSCEAR (2000)
Oka-Akoko, Nigeria (top soil)	173.00	4.84	4.84	13.00			Ajayi and Ajayi (1999)
Akunu and Ayere, Nigeria	629.28	49.96	38.58	73,00	0.364	1.273	Akingboye and Ademila (2019)
Akungba-akoko, Nigeria	831.35	45.00	33.00	60.00	1.00	0.29	UNSCEAR (2000); Tufail *et al*. (2007)
World	420.00	56.77	39.01	87.98	0.432	1.51	Akingboye *et al*. (2021)
Ilesha and environs	267.09	41.17	34.40	52.60	0.26	0.90	Present study

CHAPTER FIVE

5.0 SUMMARY, CONCLUSIONS AND RECOMMENDATIONS

5.1 Summary

Radioactivity levels and the possible radiological hazards of basement complex rocks in Ilesha and environs have been investigated in this study. It is observed that the overall average elemental and activity concentrations of ^{40}K for the study area are 2.66% and 831.35 Bq kg^{-1}; for thorium (^{232}Th) are 16 ppm and 56.77 Bq kg^{-1}; and for uranium (^{238}U) are 13.98 ppm and 39.01 Bq kg^{-1}.. The total counts emission rate (TC) has a mean value of 1597.20 cps.

The observed Radioactive Heat Production (A) for the location has values ranging from 0.69 μW m^{-3} to 5.20 μW m^{-3} with a mean value of 2.03 μW m^{-3} which is more than the global crustal A. This mean value suggests that the radioactivity process in the rocks may influence an increased heat flux experienced in the study area.

The radiological threat factors due to gamma ray from the rocks, which include mean radium equivalent activity (Raeq) of 113.85 Bq kg^{-1} is not up to the world permissible value of 370.00 Bq kg^{-1} , suggesting that the emission from the radioactive elements is negligible; the average absorbed dose of 52.60 nGy h^{-1} is below the global permissible value 60 nGy h^{-1} and within the safe limits of 28 to 120 nGy h^{-1}; the outdoor and indoor annual effective dose (AEDEout and AEDEin) estimated mean values of 0.06 and 0.26 mSv y^{-1} respectively are not up to the global limits of 0.07 mSv $y^{-1}$and 0.41 mSv y^{-1} respectively; the estimated mean for internal hazard index and external hazard index (RHex and RHin), gamma representative index (AC) and activity utilisation index (API) are not up to the permissible global permits. Thus, indicating that the study area is radiologically safe. The estimated annual gonadal effective dose (AGDE) and excessive lifetime cancer risk (ELCR) with values of 362.30 μSv y^{-1} and 9.00×10^{-4} respectively are more than the global permissible values of 300 μSv y^{-1} and 0.29×10^{-3} respectively. These call for a

reflection on applications of the rocks from the study area for building projects and similar applications. The time to time check of the radiological threat level of the location should be considered.

5.2 Conclusions

In conclusion, it was observed that the basement complex rocks in Ilesha and environs have a total counts emission rate (TC) of moderate mean value. The observed mean Radioactive thermal energy Production (RHP) per unit time is above the world crustal RHP suggesting that the radioactivity process in the rocks may influence an increased heat flux of the location.

The average radium equivalent activity (Raeq); the average absorbed dose; the indoor yearly effective dose and the outdoor yearly effective dose (AEDEout and AEDEin); the estimated averages for outside and internal threat indices (RHex and RHin), gamma representative index (AC) and activity application index (API) are not up to the recommended globe permissible values. This indicates that the emission from the radioactive elements is negligible suggesting that the environment is radiological safe.

The estimated yearly gonadal effective dose (AGDE) and excessive lifetime cancer risk (ELCR) are above the world permissible limits, pointing to the fact that there should be a drastic reduction in the use of rocks in the area for building projects and similar applications.

5.3 Recommendations

(i) Airborne radiometric data of the location was used in this work. Other methods can be used where this did not perform best.

(ii) Only few towns were considered in this work. It is therefore proposed that future work may require the use of more than one state.

REFERENCES

Abdo, A. A., Ackermann, M., Ajello, M., Atwood, W. B., Axelsson, M., Baldini, L., ... & Tanaka, T. (2009). Fermi LAT observation of diffuse gamma rays produced through interactions between local interstellar matter and high-energy cosmic rays. *The Astrophysical Journal*, *703*(2), 1249.

Achola, S. O. (2009). *Radioactivity and elemental analysis of carbonatite rocks from parts of Gwasi area, South Western Kenya* (Doctoral dissertation, University of NAIROBI).

Adabanija, M. A., Anie, O. N., & Oladunjoye, M. A. (2020). Radioactivity and gamma ray spectrometry of basement rocks in Okene area, southwestern Nigeria. *NRIAG Journal of Astronomy and Geophysics*, *9*(1), 71-84.

Adesipo, A. A., Akinbiola, S., Awotoye, O. O., Salami, A. T., & Freese, D. (2020). Impact of mining on the floristic association of gold mined sites in Southwest Nigeria. *BMC Ecology*, *20*(1), 1-13.

Aisabokhae, J., and Adeoye, M. (2020). Spatial distribution of radiogenic heat in the Iullemmeden basin–Precambrian basement transition zone, NW Nigeria. *Geology, Geophysics and Environment*, *46*(3), 238-238.

Ajayi, I. R., & Ajayi, O. S. (1999). Estimation of absorbed dose rate and collective effective dose equivalent due to gamma radiation from selected radionuclides in soil in Ondo and Ekiti State, south-western Nigeria. *Radiation protection dosimetry*, *86*(3), 221-224.

Akingboye AS, Ademila O (2019) In situ natural radioactivity and radiological hazard assessments of granite gneiss outcrops in parts of the Southwestern Basement Complex of Nigeria. J Nat Hazards and Environ 5(2):1–11. https://doi.org/10.21324 /dacd.475998

Akingboye, A. S., Ogunyele, A. C., Jimoh, A. T., Adaramoye, O. B., Adeola, A. O., and Ajayi, T. (2021). Radioactivity, radiogenic heat production and environmental radiation risk of the Basement Complex rocks of Akungba-Akoko, southwestern Nigeria: insights from in situ gamma-ray

spectrometry. *Environmental Earth Sciences*, *80*(6), 1-24.

Akinwumiju, A. S., & Olorunfemi, M. O. (2019). Development of a conceptual groundwater model for a complex basement aquifer system: The case OF OSUN drainage basin in southwestern Nigeria. *Journal of African Earth Sciences*, *159*, 103574.

Ali, K. A. A. (2015). Investigation of ^{232}Th, ^{40}K, and ^{238}U radioactivity concentrations in soil samples Port Sudan Town, Red Sea State.

Anusha, B., Kumar, D. S., Ghosh, S. O. M. S. U. B. H. R. A., Parthiban, N., Banji, D. A. V. I. D., & Goje, A. R. J. U. N. (2011). Gamma ray spectroscopy—An overview. *Int. J. Adv. Pharm. Sci*, *2*, 91-101.

Asere, A. M., & Sedara, S. O. (2020). Determination of Natural Radioactivity Concentration and Radiogenic Heat Production in Selected Quarry Sites in Ondo State, Nigeria. *NIPES J. Sci. Tech. Res*, *2*, 256.

Beretka J, Mathew PJ (1985). Natural radioactivity of Australia building materials, industrial wastes and by-products. Health phy 48:87 – 95.

Bolarinwa, A. T., & Adepoju, A. A. (2017). Geochemical characteristics and tectonic setting of amphibolites in Ifewara area, Ife-Ilesha schist belt, southwestern Nigeria. *Earth Sci Res*, *6*, 43.

Boone, J. M. (2000). X-ray production, interaction, and detection in diagnostic imaging. *Handbook of medical imaging*, *1*, 1-78.

Chandrasekaran, A., Ravisankar, R., Senthilkumar, G., Thillaivelavan, K., Dhinakaran, B., Vijayagopal, P., Bramha SN., and Venkatraman, B. (2014). Spatial distribution and lifetime cancer risk due to gamma radioactivity in Yelagiri Hills, Tamilnadu, India. *Egyptian Journal of basic and applied sciences*, *1*(1), 38-48.

Connor, D., Martin, P. G., & Scott, T. B. (2016). Airborne radiation mapping: overview and application of current and future aerial systems. *International journal of Remote Sensing*, *37*(24), 5953-5987.

El-Gamal, A., Nasr, S., El-Taher, A., (2007). Study of the spatial distribution of

natural radioactivity in Upper Egypt Nile River sediments. Rad Meas 42:457 - 465 Radiometric mapping for naturally occurring radioactive materials (NORM) assessment in Mamuju, West Sulawesi. *Atom Indonesia*, *40*(1), 33-39.

Erbek E, Dolmaz MN (2018) In situ measurements of radionuclide concentrations in south of Mulgacity, Turkey. Environ Earth Sci 77: 366–377.

European Commission EC (1999). Radiological Protection Principles concerning the Natural Radioactivity of Building Materials. Radiation Protection 112.

Faweya, E. B., & Adewumi, T. (2021). Excessive-life time cancer risks due to concentration of radionuclides and quantification of contamination of sediments from dredged portion of Niger River Nigeria. *International Journal of Radiation Research*, *19*(2), 309-316.

Gaafar, I., Abu El Ghar, M., Ibrahim, T., & Diab, M. (2020). Mineralogy and ground gamma-ray spectrometric investigation for phosphates of Gabal Abu Had area, Central Eastern Desert, Egypt. *NRIAG Journal of Astronomy and Geophysics*, *9*(1), 375-392.

IAEA (1991) Airborne gamma ray spectrometer surveying. International Atomic Energy Agency. Technical Report Series, No. 323

IAEA (2003) Radiation protection and the management of radioactive waste in the oil and gas industry. International Atomic Energy Agency. Vienna, p 173

ICRP (1977) Recommendations of the International Commission on Radiological Protection (ICRP). Pergamon press, New York, p 87

ICRP (1990) Recommendations of the International Commission on Radiological Protection (ICRP). Pergamon press, New York, p 60 (ICRP Pub)

Ibeanu, I. G. E. (2003). Tin mining and processing in Nigeria: cause for concern?. *Journal of environmental radioactivity*, *64*(1), 59-66.

Idriss, H., Salih, I., Alaamer, A. S., Al-Rajhi, M. A., Osman, A., Adreani, T. E., Abdelgalil, M. Y., & Ali, N. I. (2018). Health risk profile for terrestrial radionuclides in soil around artisanal gold mining area at Alsopag,

Sudan. *Acta Geophysica*, *66*(4), 673-681.

Innocent, A.J, Onimisi, M.Y., & Jonah, S.A. Evaluation of naturally occurring radionuclide materials in soil samples collected from some mining sites in Zamfara State, Nigeria. British Journal of Applied Science & Technology, 2013; 3(4), 684-692.

Kayode, J. S., Nyabese, P., & Adelusi, A. O. (2010). Ground magnetic study of Ilesa east, Southwestern Nigeria. *African Journal of Environmental science and technology*, *4*(3).

Maden N, Akaryali E (2015a). Gamma ray spectrometry for recognition of hydrothermal alteration zones related to a low sulfidation epithermal gold mineralisation (eastern Pontides, NE Turkiye). J Appl Geophys 122:74 – 85.

Maden N, Akaryali E (2015b). A review for genesis of continental arc magmas: U, Th, K and radiogenic heat production data from the Gumushane Pluton in the Eastern Pontides (NE Turkiye). Tectonophys 664:225 – 243.

Madhav, S., Ahamad, A., Singh, A. K., Kushawaha, J., Chauhan, J. S., Sharma, S., & Singh, P. (2020). Water pollutants: sources and impact on the environment and human health. *Sensors in Water Pollutants Monitoring: Role of Material*, 43-62.

Mamont-Ciesla K, Gwiazdowski B, Biernacka M, Zak A (1982). Radioactivity of buiding materials in Poland. In: Vohra G, Pillai KC, Sadavisan S (eds) Natural radiation environment. Halsted Press, New York, p 551.

Mareschal JC, Jaupart C, Gariepy C, Cheng LZ, Guillou-Frottier L, Bienfait G, Lapointe R (2000). Heat flow and deep thermal structure near the southeastern edge of the Canadian Shield. Can J Earth Sci 37:399 – 414.

Minty, B. R. S. (1997). Fundamentals of airborne gamma-ray spectrometry. *AGSO Journal of Australian Geology and Geophysics*, *17*, 39-50.

NGSA (2009) Sources, Nigeria Geological Survey Agency (2009).

Oyinloye, A. O. (2006). Metallogenesis of the lode gold deposit in Ilesha area of

southwestern Nigeria: inferences from lead isotope systematics. *Biological Sciences-PJSIR*, *49*(1), 1-11.

Rafque M, Rahman SU, Basharat M, Aziz W, Ahmad I, Lone KA, Ahmad K, Matiullah (2014) Evaluation of excess life time cancer risk from gamma dose rates in Jhelum valley. J Rad Res Appl Sci.

Ramasamy V, Suresh G, Meenakshisundaram V, Gajendran V (2009). Evaluation of natural radionuclide content in river sediments and excess lifetime cancer risk due to gamma radioactivity. Res J Environ Earth Sci 1(1): 6 – 10.

Ramasamy V, Suresh G, Meenakshisundaram V, Ponnusamy V (2011). Horizontal and vertical characterisation of radionuclides and minerals in river sediments. App Rad Isotopes 69(1): 184 – 195.

Reguigui, N. (2006). Gamma ray spectrometry. *Practical Information*, *21*.

Rizwan, U. (2015). *Development of Gamma-Ray Spectroscopy Techniques for Fundamental and Applied Research* (Doctoral dissertation, Science: Department of Chemistry).

Rosianna, I., Nugraha, E. D., Syaeful, H., Putra, S., Hosoda, M., Akata, N., & Tokonami, S. (2020). Natural radioactivity of laterite and volcanic rock sample for radioactive mineral exploration in Mamuju, Indonesia. *Geosciences*, *10*(9), 376.

Rybach L (1988). Determination of the heat production rate. In: Haenel R, Rybach L, Stegena L (eds). Handbook of terrestrial heat-flow density determination. Kluwer Academic Publishers, Dordrecht, pp 125 - 142.

Semenova, Y., Pivina, L., Zhunussov, Y., Zhanaspayev, M., Chirumbolo, S., Muzdubayeva, Z., & Bjørklund, G. (2020). Radiation-related health hazards to uranium miners. Environmental Science and Pollution Research, 27(28), 34808-34822.

Syaeful, H., Sukadana, I. G., & Sumaryanto, A. (2014). Radiometric mapping for naturally occurring radioactive materials (NORM) assessment in Mamuju, West Sulawesi. *Atom Indonesia*, *40*(1), 33-39.

Tallini, A. (2011). Health is state of physical, mental, and social wellbeing. *BMJ: British Medical Journal (Online)*, *343*.

Tan G, Li C, Li M (1991) Investigation of environment natural penetrating radiation level in Guangdong Province. Rad io Protection 11:47–57 (in Chinese with English abstract)

Taskin, H., Karavus, M., Ay P., Topuzoglu A., Hindiroglu, S., Karahan, G. (2009). Radionuclide concentration in soil and lifetime cancer risk due to gamma radioactivity in Kirklareli, Turkey. J Environ Radio 100(1):49 – 53.

Tufail M, Nasim-Akhar Sabiha-Javied SA, Hamid T (2007) Natural radiation hazard in building bricks fabrication from soils of two districts of Pakistan. J Radio Protection 27:481–492.

Terrill, J. G., & Moeller, D. W. (1954). *Concepts of Radiological Health* (No. 336). US Department of Health, Education, and Welfare, Public Health Service, Radiological Health Branch.

UNSCEAR (1988) Sources, effects and risks of ionizing radiation. United Nations Scientific Committee on Effect of Atomic Radiation (UNSCEAR). United Nations, New York, p 647.

UNSCEAR (1993) Sources and effects of ionizing radiation. United Nations Scientific Committee on Effect of Atomic Radiation (UNSCEAR). United Nations, New York, p 920.

UNSCEAR (2000) Exposure from natural radiation source. United Nations Scientific Committee on Effect of Atomic Radiation (UNSCEAR), Report to general assembly. Annex B. United Nations, New York, p 76.

UNSCEAR, Sources, effects, and risks of ionization radiation. United Nations Scientific Committee on the Effects of Atomic Radiation, Report to the General Assembly, with Annexes, 2000, New York.

Weldeslassie, T., Naz, H., Singh, B., & Oves, M. (2018). Chemical contaminants for soil, air and aquatic ecosystem. In *Modern age environmental problems and their remediation* (pp. 1-22). Springer, Cham.

Xinwei, L., Lingqing, W., & Xiaodan, J., (2006). Radiometric analysis of Chinese commercial granites. J Radioanalytical Nuclear Chem 267(3):669 – 673.

Youssef, M.A.S., (2016). Estimating and interpretation of radioactive heat production using airborne gamma ray survey data of Gabal Arrubushi area, Central Eastern Desert, Egypt. J Afr Earth Sci. 1:1.